RESEARCH ARTICLE

BJP — BRITISH PHARMACOLOGICAL SOCIETY

Combined targeting of fatty acid amide hydrolase and melatonin receptors promotes neuroprotection and stimulates inflammation resolution in rats

Mariarosaria Cammarota[1] | **Francesca Ferlenghi**[2] | **Federica Vacondio**[2] |
Fabrizio Vincenzi[3] | **Katia Varani**[3] | **Annalida Bedini**[4] | **Silvia Rivara**[2] |
Marco Mor[2] | **Francesca Boscia**[1]

[1]Division of Pharmacology, Department of Neuroscience, Reproductive Sciences and Dentistry, School of Medicine, Federico II University of Naples, Naples, Italy

[2]Department of Food and Drug, University of Parma, Parma, Italy

[3]Department of Translational Medicine, University of Ferrara, Ferrara, Italy

[4]Department of Biomolecular Sciences, University of Urbino 'Carlo Bo', Urbino, Italy

Correspondence
Francesca Boscia, Division of Pharmacology, Department of Neuroscience, Reproductive Sciences and Dentistry, School of Medicine, Federico II University of Naples, Via Sergio Pansini 5, 80131 Naples, Italy.
Email: boscia@unina.it

Background and Purpose: Devising novel strategies to therapeutically favour inflammation resolution and provide neuroprotection is an unmet clinical need. Enhancing endocannabinoid tone by inhibiting the catabolic enzyme fatty acid amide hydrolase (FAAH), or stimulating melatonin receptors has therapeutic potential to treat neuropathological states in which neuroinflammation plays a central role.

Experimental Approach: A rodent hippocampal explant model of inflammatory injury was used to assess the effects of UCM1341, a dual-acting compound with FAAH inhibitory action and agonist activity at melatonin receptors, against neuroinflammatory damage. FAAH activity was measured by a radiometric assay, and N-acylethanolamine levels were assessed by HPLC–MS/MS methods. FAAH distribution, evolution of inflammation and the contribution of UCM1341 to the expression of proteins controlling macrophage behaviour were investigated by biochemical and confocal analyses.

Key Results: UCM1341 exhibited greater neuroprotection against neuroinflammatory degeneration, compared with the reference compounds URB597 (FAAH inhibitor) and melatonin. During neuroinflammation, UCM1341 augmented the levels of anandamide and N-oleoylethanolamine, but not N-palmitoylethanolamine, up-regulated PPAR-α levels, attenuated demyelination and prevented the release of TNF-α. UCM1341 modulated inflammatory responses by contributing to microglia/macrophage polarization, stimulating formation of lipid-laden macrophages and regulating expression of proteins controlling cholesterol metabolism and efflux. The neuroprotective effects of UCM1341 were prevented by PPARα, TRPV1 and melatonin receptor antagonists.

Conclusion and Implications: UCM1341, by enhancing endocannabinoid and melatoninergic signalling, benefits neuroprotection and stimulates inflammation resolution pathways. Our findings provide an encouraging prospect of therapeutically targeting

---

Abbreviations: ABCA1, ATP-binding cassette transporter member 1; AD, Alzheimer's disease; AEA, anandamide; BCA, bicinchoninic acid; BSA, bovine serum albumin; DAM, disease-associated microglia; DIV, days in vitro; EAE, experimental autoimmune encephalomyelitis; FAAH, fatty acid amide hydrolase; GFAP, glial fibrillary acidic protein; GSSG, glutathione disulfide; HBSS, Hank's balanced salt solution; HPLC–MS/MS, high-performance liquid chromatography coupled to tandem mass spectrometry; HS, horse serum; LXR, liver X receptor; MAP2, microtubule-associated protein 2; MBP, myelin basic protein; MEM, minimal essential medium; MS, multiple sclerosis; NF200, neurofilament 200; NM, normal medium; OEA, N-oleoylethanolamine; PEA, N-palmitoylethanolamine; PI, propidium iodide; Plin2, perilipin2; SFM, serum-free medium; TREM2, triggering receptor expressed on myeloid cells-2.

---

1 | INTRODUCTION

Neuroinflammation is a critical determinant for the pathogenesis of several neurodegenerative disorders and chronically contributes to glial dysfunction, neuronal death and remyelination failure in multiple sclerosis (MS) or Alzheimer's disease (AD) (Franklin & Ffrench-Constant, 2017). Promoting neuroprotection and modulating the microglia/macrophage response are important therapeutic goals to accelerate myelin repair, improve functional recovery and prevent disease progression (Boscia et al., 2021).

Endocannabinoids are lipid mediators released on demand from membrane phospholipid precursors exerting their effects via the activation of cannabinoid CB_1/CB_2 receptors and non-cannabinoid receptors, including the **peroxisome proliferator-activated receptors** (PPARs), **transient receptor potential vanilloid type 1** (TRPV1) and other G protein-coupled receptors (GPCRs), including **GPR55**, **GPR18** and **GPR119** (Irving et al., 2017). Inhibition of the endocannabinoid-hydrolysing enzyme **fatty acid amide hydrolase** (FAAH) increases the levels of biologically active endocannabinoid and related ethanolamides, including **anandamide** (AEA), **N-oleoylethanolamine** (OEA) and **N-palmitoylethanolamine** (PEA) (Kathuria et al., 2003). Although AEA is an endocannabinoid, the other ethanolamides exert their activity through non-cannabinoid receptors, such as **PPAR-α** and GPR119, sustaining the immunomodulatory and neuroprotective activity (Petrosino & Di Marzo, 2010; Piomelli, 2003). The pharmacological inhibition of FAAH is considered a valuable therapeutic approach to treat depression and anxiety disorders, also when they are co-morbid conditions of chronic inflammatory diseases (Bortolato et al., 2007; Kathuria et al., 2003; Vecchiarelli et al., 2021). Targeting FAAH also represents a promising treatment option to enhance anti-nociceptive and anti-inflammatory effects and provide neuroprotection (Piomelli & Mabou Tagne, 2022).

The indoleamine **melatonin**, (*N*-acetyl-5-methoxytryptamine), the main neurohormone of the pineal gland, regulates the sleep–wake cycle and other physiological functions acting via non-receptor and receptor-dependent signalling pathways (Liu et al., 2019). In the mammalian brain, melatonin receptor-dependent effects result from the activation of two GPCRs, the melatonin receptor type 1 (MT_1) and melatonin receptor type 2 (MT_2), that exist as homodimers and/or heterodimers with themselves or other GPCRs, such as **GPR50** (Jockers et al., 2016). Even if the cytoprotective effect of melatonin has been often related to its free radical scavenging activity, due to the presence of the indole ring, increasing evidence highlights an important role of its receptor activity for antioxidant,

What is already known

- Enhancing the endocannabinoid and melatoninergic tone has therapeutic potential to treat neuroinflammatory diseases.
- UCM1341 is a dual-acting compound with FAAH inhibitory action and agonist activity on melatonin receptors.

What does this study add

- UCM1341 protected against neuroinflammatory degeneration and stimulated inflammation resolution pathways in neonatal rat hippocampal tissue.
- Activation of PPAR-α, TRPV1 channels and melatonin receptors contributes to the beneficial effects of UCM1341.

What is the clinical significance

- FAAH inhibition and activation of melatonin receptors provide synergistic neuroprotection against the neuroinflammatory damage.
- Our findings provide an encouraging prospect of targeting endocannabinoid and melatoninergic systems in inflammatory states.

immunomodulatory and neuroprotective roles through the activation of the **nuclear erythroid 2-related factor 2 (Nrf2)** pathway and suppression of pro-inflammatory NF-κB signalling (Nikolaev et al., 2021).

Recently, our research group has developed dual-acting compounds, with potent and balanced FAAH inhibitory action and agonist activity on melatonin receptors (Spadoni et al., 2018). Among them, UCM1341, having nanomolar MT_1/MT_2 binding affinity and inhibitory potency on FAAH, was able to reduce intraocular pressure, an effect exerted by both melatonin and FAAH substrates, including the endocannabinoid AEA, with improved activity compared to single agents.

In the present study, we investigated whether FAAH inhibition combined with the activation of melatonin receptors may represent a synergistic drug combination to provide neuroprotection.

To this aim, we tested the effects of UCM1341 and the reference compounds, melatonin and URB597 (an established FAAH inhibitor), alone or in combination, against N-methyl-D-aspartate (NMDA)-induced excitotoxicity or lipopolysaccharide (LPS) + interferon-γ (IFN-γ)-induced neuroinflammatory damage in rat hippocampal explant cultures. UCM1341 exerted a greater neuroprotection against the neuroinflammatory insult, compared with those of the reference compounds, melatonin and URB597. UCM1341 also modulated the inflammatory response by contributing to microglia/macrophage polarization and regulating the expression of proteins controlling cholesterol metabolism and efflux. Collectively, our findings demonstrated a synergistic contribution of both endocannabinoid and melatoninergic signalling to the beneficial effects of the bivalent ligand during neuroinflammation.

2 | METHODS

2.1 | Animals

Animal studies are reported in compliance with the ARRIVE guidelines (Piercie du Sert., 2020) and with the recommendations made by the British Journal of Pharmacology (Lilley et al., 2020). All animal experiments and animal handling and care were in accordance with the Guide for the Care and Use of Laboratory Animals (EU Directive 2010/63/EU), and the experimental protocol was approved by the Animal Care and Use Committee of 'Federico II' University of Naples, Italy, and Ministry of Health, Italy (#515/2019-PR). Female Wistar rats (14 days timed pregnant) were obtained from Charles River Laboratories (Calco, Italy) and maintained at a constant temperature (22 ± 1°C) on a 12 h light/dark cycle (lights on at 7:00 AM) with food and water ad libitum. Welfare-related assessments were carried out serially during the study. All efforts were made to minimize animal suffering and to reduce the number of animals used. The pregnant dams were allowed to deliver their pups naturally. At 7–9 days postpartum, littermates weighing 15–20 g were used for the preparation of organotypic explants. Both male and female animals were used for organotypic explant preparation.

2.2 | Hippocampal organotypic explants

Organotypic explants were prepared as previously described (Boscia et al., 2006, 2008). Postnatal P7- to P9-day-old Wistar rat pups were killed by cervical dislocation, and 400-μm-thick parasagittal slices were obtained from dissected hippocampi using a McIlwain tissue chopper (Campden Instruments, Leicester, UK) and placed into ice-cold Hank's balanced salt solution (HBSS, Gibco, Milan, Italy, Cat# 24020117) supplemented with 5 mg·ml^{-1} glucose and 1.5% (v/v) fungizone. Cultures were then transferred to a humidified semiporous membrane (30 mm Millicell tissue culture plate inserts of 0.4 m pore size from Millipore, Milan, Italy, Cat# PICM03050) in six-well tissue culture plates (five slices per membrane). Each well contained 1.2 ml of tissue culture medium consisting of 50% minimal essential medium (MEM, Gibco, Milan, Italy, Cat# 11095080), 25% HBSS, 25% heat-inactivated horse serum (HS, Gibco, Italy, Cat# 26050088), 6.5 mg·ml^{-1} glucose, 1 mM glutamine and 1.5% fungizone (Thermo Fisher Scientific, Italy, Cat# 15290018) (normal medium [NM]). Cultures were maintained at a 37°C and 5% CO_2-conditioned atmosphere. Experiments were performed on cultures kept in vitro for 7 days (7 DIV) or 10 days (10 DIV).

Therapeutic screens in organotypic explant cultures prepared from rodent postnatal P7–P9 brains provide a valuable system to study candidate lead compounds for neuroprotection and their mechanism of action in a multicellular CNS context. Brains of postnatal animals are commonly used for slice cultures because they are more resistant to mechanical trauma that occurs during the slice preparation compared to the adult brains. Preparing organotypic brain slice cultures from adult brains is more challenging and requires to be optimized for long-term culturing such as culturing at lower temperatures, optimizing culture medium components or reducing the thickness because the cell survival is very limited and cytoarchitectural organization of the tissue is not retained for a long time (Boscia et al., 2008).

2.3 | NMDA-induced neurodegeneration and drug exposure

Treatment with NMDA was carried out in hippocampal cultures, as previously described (Boscia et al., 2006). Organotypic hippocampal slice cultures were removed from NM, washed in SFM and exposed to 10–30 μM NMDA (with or without test compounds) for 48 h in fresh SFM. Control hippocampal cultures were kept in SFM. Appropriate concentrations of UCM1341 (0.1–10 μM), URB597 (10 μM), melatonin (10 μM) or vehicle (DMSO ≤ 0.1%) were added to the medium at the beginning of the treatment and were kept in the culture medium during the entire duration of the experiment.

2.4 | LPS + IFN-γ-induced neurodegeneration and drug exposure

Hippocampal explants were removed from normal serum-containing medium, washed in SFM (consisting of NM with serum replaced with MEM, plus 1% HS) and exposed to a combined application of 10 μg·ml^{-1} LPS + 100 ng·ml^{-1} IFN-γ for 72–96 h in SFM. This model, by mimicking microglial interaction with infiltrating peripheral immune T cells, triggers the release of large amounts of pro-inflammatory and cytotoxic factors and promotes an inflammatory neurodegeneration (Papageorgiou et al., 2016). Appropriate concentrations of UCM1341 (0.1–10 μM), URB597 (10 μM), melatonin (10 μM) or vehicle (DMSO ≤ 0.1%) were added to the medium at the beginning of the treatment and were kept in the culture medium during the entire duration of the experiment. Luzindole, a melatonin receptor antagonist (0.1–10 μM), AM251, a CB$_1$ receptor antagonist (0.1–10 μM), AM630, a CB$_2$ receptor antagonist (0.1–10 μM), SB3667, a TRPV1 channel antagonist (0.03–10 μM) or GW6471, a PPARα antagonist

(10 μM) were added to the cultures for 1 h before treatment with the LPS/IFN-γ combination and used at concentrations that had no effect when used alone (Landucci et al., 2021). Control culture explants were kept in SFM, in the absence or presence of test compounds.

2.4.1 | Assessment of cell death and image analysis

Cell injury was assessed in explants by live incorporation of a marker of compromised membrane integrity, PI (5 μg·ml^{-1}), that emits a bright red fluorescence when exposed to blue–green light. For densitometric measurements, the digital pictures were analysed with the Image-Pro Plus software (Media Cybernetics), after freehand outlining of the cornu ammonis (CA) neuronal layer, as previously described (Boscia et al., 2006, 2008).

2.5 | Immunoblotting

Explant extract preparation and immunoblotting were performed as previously described (Boscia et al., 2015). The slices were lysed in 50 mM Tris–HCl pH 8.0 buffer containing 150 mM NaCl, 1% Nonidet P-40, 2 μg·ml^{-1} aprotinin, 1 μg·ml^{-1} pepstatin, 2 μg·ml^{-1} leupeptin and 1 mM Na$_3$VO$_4$. Protein concentration was determined by the Bradford assay using BSA as the standard, and the crude extracts were analysed with 8% or 14% SDS–polyacrylamide gel. Then, gels were electrophoretically transferred onto nitrocellulose membranes, and filters were probed with the indicated primary antibodies: rabbit polyclonal anti-FAAH (1:5000, Cayman Chemical, Ann Arbor, MI, USA, RRID:AB_327842), rabbit polyclonal anti-Iba1 (1:2000, Wako Chemicals, USA, Cat# 019-19741), mouse monoclonal anti-MEL-1A/B-R (1:1000, Santa Cruz Biotechnology, Inc., Dallas, TX, USA, RRID:AB_2833090), rat monoclonal anti-myelin basic protein (MBP, 1:1000, Merck Life Science S.r.l., Milan, Italy, RRID:AB_240845), rabbit polyclonal anti-mannose receptor CD206 (1:5000, Abcam, RRID:AB_10896526), rabbit polyclonal anti-**arginase-1** (Arg-1, 1:5000, Abcam, Cambridge, UK, RRID:AB_10563668), rabbit polyclonal anti-AMP-activated protein kinase (**AMPK**) and anti-phospho-AMPK (1:1000, each, Cell Signaling, Danvers, MA, USA, RRID:AB_310416, RRID:AB_390759), mouse monoclonal anti-triggering receptor expressed on myeloid cells-2 (TREM2, 1: 1500, Santa Cruz Biotechnology, Inc., Dallas, TX, USA, RRID:AB_1130660), mouse monoclonal anti-liver X receptor α/β 1:300 (**LXR**α/β, Santa Cruz Biotechnology, Inc., Dallas, TX, USA, RRID:AB_2251583), mouse monoclonal anti-ATP-binding cassette transporter member 1 (**ABCA1**; 1:1000, Santa Cruz Biotechnology, Inc., Dallas, TX, USA, RRID:AB_830977), mouse monoclonal anti-PPARα (1:600, Santa Cruz Biotechnology, Inc., Dallas, TX, USA, RRID:AB_2165759) and rabbit polyclonal anti-β-actin (1:1000, Merck Life Science S.r.l., Milan, Italy, RRID:AB_476744). Proteins were visualized with peroxidase-conjugated secondary antibodies, using the enhanced chemiluminescence system (Amersham Pharmacia Biosciences Ltd, Uppsala, Sweden, Cat# RPN2209). Films were scanned, and the signal ratio of (protein of interest/

housekeeping protein) was quantified densitometrically. Where indicated, filters were stripped as described (Cammarota et al., 2021). The immuno-related procedures used comply with the recommendations made by the British Journal of Pharmacology (Alexander et al., 2018).

2.6 | Confocal microscopy

Confocal immunofluorescence procedures in organotypic explants were performed as previously described (Boscia et al., 2013; de Rosa et al., 2019). Slices were fixed in 4% w/v paraformaldehyde in phosphate buffer (PB) for 1 h, blocked with 3% BSA and 0.05% Triton X (Merck Life Science S.r.l., Milan, Italy, Cat# 9036-19-5) for 40 min and then incubated with the following primary antibodies: rabbit polyclonal anti-FAAH (1:1500, Cayman Chemical, Ann Arbor, MI, USA, RRID:AB_327842), mouse monoclonal anti-glial fibrillary acidic protein (GFAP) (1:1000, Merck Life Science S.r.l., Milan, Italy, RRID:AB_10013721), rabbit polyclonal anti-Iba1 (1:2000, Wako Chemicals, USA, Cat# 019-19741), mouse monoclonal anti-CD11b (1:1000, Thermo Fisher Scientific, Inc., RRID:AB_2536484), mouse monoclonal anti-microtubule-associated proteins MAP2 (1:2000, Merck Life Science S.r.l., Milan, Italy, RRID:AB_91939), rabbit polyclonal anti- neurofilament-200 (anti-NF200; 1:500, Merck Life Science S.r.l., Milan, Italy, RRID:AB_1842647), rat monoclonal anti-MBP (1:1000, Merck Life Science S.r.l., Milan, Italy, Cat# MAB386), rabbit polyclonal anti-CD206 (1:13,000, Abcam, Cambridge, UK, RRID:AB_10896526), guinea pig polyclonal anti-GABA (1:400, Merck Life Science S.r.l., Milan, Italy, RRID:AB_213533), guinea pig polyclonal anti-perilipin2 (Plin2; 1:3000, Progen, Heidelberg, Germany, RRID:AB_2895086) and mouse monoclonal anti-ABCA1 (1:400, Santa Cruz Biotechnology, Inc., Dallas, TX, USA, RRID:AB_830977). After 48 h at 4°C, slices were incubated with the corresponding secondary antibodies for 2 h at room temperature. Finally, they were mounted on glass slides and imaged with Zeiss LSM 700 laser (Carl Zeiss, Jena, Germany) scanning confocal microscope.

Controls of the methods included replacement of the primary antisera with normal serum (1:200). To control for a possible cross-reactivity between IgGs in double immunolabelling experiments, some sections were processed through the same immunocytochemical sequence except that primary antisera were replaced with normal serum, or only one primary antibody was applied, but the full complement of secondary antibodies was maintained. In addition, the secondary antibodies utilized were highly pre-adsorbed to the IgGs of numerous species. Tissue labelling without primary antibodies was also tested to exclude autofluorescence. No specific staining was observed under these control conditions, thus confirming the specificity of the immunosignals.

2.6.1 | Quantification of confocal studies in hippocampal explants

Confocal microscopy was used to obtain stacks of photographs of FAAH/MAP2, FAAH/GFAP, FAAH/CD11b and MBP/NF200

immunolabelling at 2 μm intervals in the CA1 area at 40× magnification and a resolution of 1024 × 1024, between a depth of 5–20 μm from the upper surface. Four slices were analysed per condition in each experimental session. Five images of randomly chosen areas of each slice were acquired with identical fluorescence intensity. Maximum intensity projection (MIP) images were created for each stack by using ZEN imaging software. Then, for each MIP image, the quantification of colocalization between FAAH and MAP2, FAAH and GFAP, FAAH and CD11b, and MBP with NF200 immunostaining was assessed by using the 'co-localization highlighter' plug-in for the ImageJ software (NIH, Bethesda, MD, USA) (de Rosa et al., 2019). Before co-localization analysis, images were first thresholded to identify the positive signal. Subsequently, the number of pixels positive for FAAH/MAP2, FAAH/GFAP, FAAH/CD11b and MBP/NF200 was measured per microscope field. This value, expressed as percentage of co-localization, represents the extent of FAAH/MAP2, FAAH/GFAP, FAAH/CD11b and MBP/NF200 co-expression.

Quantification of immunofluorescence intensities was quantified in terms of pixel intensity by using the Image J software (NIH, Bethesda, MA, USA), as described previously (Casamassa et al., 2016). Digital images were taken with 40× objective, and identical laser power settings and exposure times were applied to all the photographs from each experimental set.

The number of GABA⁺ and CD206⁺ cells as well as double-labelled Iba1⁺/Plin2⁺ or Iba1⁺/ABCA1⁺ cells was determined in the CA1 pyramidal region by manual counting at 40× or 60× magnification. Only cells with a clearly visible cell body and profiles were counted.

Microglial cell morphology in the CA1 pyramidal layer was evaluated with Iba1 immunostaining (Boscia et al., 2009). Individual Iba1⁺ cells were scored according to their morphology in four main categories: (i) *surveillant and intermediate*, including microglia characterized by small cell bodies and radial thin processes (surveillant) or larger/elongated cell body and shorter thick processes (intermediate); (ii) *amoeboid*, including spherical cells with or without very short processes; (iii) *foamy*, having a vacuolated bubbly cytoplasm; and (iv) *dystrophic*, characterized by twisted and fragmented processes. Quantification of cell surface area occupied by GFAP protein was performed with ImageJ using the application: threshold from background, followed by manually defining the area and finally measuring the area fraction above the threshold.

2.7 | Quantification of IL-6, IL-10 and TNF-α

Levels of IL-6, IL-10 and TNF-α were determined with specific quantitative sandwich ELISA kits following the manufacturers' instructions (Thermo Fisher Scientific, Inc, Waltham, MA, USA, IL-6 Cat# BMS625, IL-10, Cat# BMS629; TNFα, Elabscience, Houston, TX, USA, Cat# E-EL-R2856). The reaction was developed with streptavidin–horseradish peroxidase, and the optical density was measured spectrophotometrically at a wavelength of 450 nm in a PerkinElmer EnSight Multimode Plate Reader (Vincenzi et al., 2017). Experiments for TNF-α quantification were performed in duplicate.

2.8 | Quantification of *N*-acylethanolamines in hippocampal cultures

The *N*-acylethanolamines - AEA, OEA and PEA - were extracted from hippocampal tissue homogenates by protein precipitation via acetonitrile addition, as previously reported (Carnevali et al., 2020). Briefly, five hippocampal tissue slices (100 μm thick) were homogenized in 100 μl of Tris buffer (50 mM, pH 7.5, 4°C) containing 0.32 M sucrose. Two volumes of acetonitrile, containing 100 nM AEA-d$_4$, OEA-d$_4$ and PEA-d$_4$ as internal standards, were added, and, after centrifugation (16,000 g, 10 min, 4°C), levels of *N*-acylethanolamines were quantified by HPLC coupled to tandem mass spectrometry (HPLC–MS/MS). Compound-dependent parameters were optimized by flow injection analysis of 5 μM standard solutions in methanol. Acquisition occurred in positive ion (ESI⁺) and in multiple-reaction monitoring (MRM) mode. For quantitative analysis, the following parent–product ion transitions were selected: AEA: m/z 348.2 [M + H]⁺ → m/z 90.9 + m/z 62.1 (tube lens [TL]: 54 V; collision energy [CE]: 42 and 14 eV, respectively); AEA-d$_4$: m/z 352.2 [M + H]⁺ → m/z 202.8 + m/z 66.3 (TL: 76 V; CE: 12 and 17 eV); OEA: m/z 326.3 [M + H]⁺ → m/z 309.3 + m/z 93.3 + m/z 62.3 (TL: 115 V; CE: 10, 19 and 28 eV); OEA-d$_4$: m/z 330.1 [M + H]⁺ → m/z 313.4 + m/z 66.2 (TL: 67 V; CE: 14 and 15 eV); PEA: m/z 300.3 [M + H]⁺ → m/z 62.3 (TL: 54 V; CE: 14 and 42 eV); and PEA-d$_4$: m/z 304.2 [M + H]⁺ → m/z 287.1 + m/z 66.3 (TL: 72 V; CE: 12 and 15 eV). A Waters XSelect HSS T3 column (100 × 2.1 mm, 3.5 μm particle size; Waters Corp, USA, Cat# 186006465) was employed for gradient separation (eluent A: acetonitrile + 0.1% v/v formic acid; eluent B: water + 0.1% v/v formic acid; t(0 min): 5% A:95% B; t(1 min): 5% A:95% B; t(6 min): 100% A:0% B; t(11 min): 100% A:0% B; t(12 min): 5% A:95% B, with a 3 min equilibration time; total run time: 15 min). Solvent flow was 0.22 ml·min⁻¹, and injected volume was 10 μl. Calibration curves were prepared in the 0.5–500 nM concentration range for AEA and in the 2.5–500 nM range for OEA and PEA, using 2 μl of a DMSO stock solution containing the compound mixture in 198 μl of charcoal-treated rat plasma and processing the calibration standards following the same procedure described for unknown samples. Calibration curves showed good linearity with coefficients of correlation (r^2) >0.99. The limit of quantification (LOQ) was equal to 0.5 nM for AEA and 2.5 nM for OEA and PEA. Total protein content in hippocampal tissue homogenates was quantified by the bicinchoninic acid (BCA) protein kit (Pierce Biotechnology, Rockford, IL, USA, Cat# 23225) following the supplier's protocol, and *N*-acylethanolamine content was expressed as pmol·mg⁻¹ protein.

2.9 | Determination of GSH and GSSG levels in hippocampal cultures

GSH and GSSG were measured by HPLC–MS/MS starting from hippocampal tissue homogenates obtained according to the procedure described in the previous section. Briefly, two volumes of acetonitrile containing 0.1% HCOOH were added to one volume of hippocampal

tissue homogenate. After centrifugation (16,000 x g, 10 min, 4°C), levels of GSH and GSSG were quantified by HPLC–MS/MS. A Waters XSelect HSS T3 column (100 × 2.1 mm, 3.5 μm particle size, Waters Corp, USA, Cat# 186006465) was employed for gradient separation (eluent A: acetonitrile + 0.1% v/v formic acid; eluent B: water + 0.1% v/v formic acid; gradient conditions: t(0 min): 5% A:95% B; t(3 min): 5% A:95% B; t(4 min): 100% A:0% B; t(5 min): 100% A:0% B; t (5.5 min): 5% A:95% B, with a 2.5 min equilibration time; total run time: 8 min). Solvent flow was 0.22 ml·min^{-1}, and injected volume was 10 μl. For quantitative analysis, the following parent–product ions transitions were selected: GSH m/z 308.0 [M + H]$^+$ → m/z 162.0 + m/z 84.2 + m/z 76.2 (TL: 106 V; CE: 14, 23 and 28 eV); GSSG m/z 613.1 [M + H]$^+$ → m/z 484.1 + m/z 354.9 + m/z 230.9 (TL: 138 V; CE: 17, 21 and 33 eV). Calibration curves showed good linearity in the 100 nM to 20 μM concentration range for both GSH and GSSG. GSH levels were expressed as nmol·mg^{-1} protein.

2.10 | HPLC–MS/MS system configuration

A Thermo Accela UHPLC gradient system coupled to a Thermo TSQ Quantum Max triple quadrupole mass spectrometer (Thermo, Madison, WI, USA) equipped with a heated electrospray ionization (H-ESI) ion source was employed for quantification of N-acylethanolamines, GSH and GSSG. H-ESI source tune parameters were set as follows: probe middle (D) position; capillary temperature: 270°C; and spray voltage: 4.0 kV. Nitrogen was used as nebulizing gas at the following pressure: sheath gas: 35 psi; auxiliary gas: 15 arbitrary units (a.u.). Argon was used as collision gas at a pressure of approximately 1.5 mTorr (1 Torr = 133.3 Pa). The software Xcalibur Version 2.2 (Thermo, Madison, WI, USA, RRID:SCR_014593) was employed for HPLC–MS/MS data acquisition and processing.

2.11 | FAAH activity assay

Hippocampal tissue homogenates were centrifuged (1000 g, 10 min, 4°C), and total protein content was quantified in the supernatant by the BCA protein kit. FAAH activity was measured in the samples by incubating 50 μg of protein from hippocampal homogenates with [^{3}H]-AEA (10,000 dpm) and 10 μM AEA for 30 min at 37°C in 0.5 ml Tris buffer (50 mM, pH 7.5) containing fatty acid-free BSA (0.05%, w/v), as previously reported (Clapper et al., 2009). The enzymatic reaction was stopped by addition of 1 ml of 1:1 chloroform:methanol mixture. After centrifugation (2000 x g, 10 min, 4°C), [^{3}H]-ethanolamine was measured in the aqueous phase by liquid scintillation counting.

2.12 | Data and statistical analysis

The data and statistical analysis comply with the recommendations of the British Journal of Pharmacology on experimental design and analysis in pharmacology (Curtis et al., 2018). Sample sizes for experiments (n = 5) were calculated a priori by using G*Power software in order to reach a power of 80%.

All the experiments were designed to generate groups of equal size, using randomization. Experiments were performed on 25–35 organotypic slices from at least three independent litters. From each pup, we isolated 20–25 hippocampal slices (4–5 data points) that were randomly assigned to the treatments. Results obtained for each pup were averaged and used as the experimental unit in the statistical analyses. Sample sizes are indicated in the figure legends. Group size (n) is the number of independent values or studied animals, and statistical analysis was undertaken only for studies where each group size was at least n = 5. Sample processing and quantification in microscopy studies were performed in a blinded manner. For pharmacological treatments, the investigator was not blinded to the experimental groups. In some experiments, data were normalized to reduce unwanted sources of variation. The data are expressed as the mean ± SEM of the values obtained from individual experiments. Statistical comparisons between two groups were performed by two-tailed Student's t test (for parametric data and Gaussian distribution). Statistical comparisons for multiple groups were performed by one-way ANOVA followed by Bonferroni post hoc test. GraphPad Prism 6.0 was used for statistical analysis (GraphPad Software, Inc, La Jolla, CA, USA, RRID:SCR_002798). Post hoc tests were conducted only if F in ANOVA achieved $P < 0.05$ and there was no significant variance in homogeneity. *$P < 0.05$ was considered the threshold for statistical significance.

2.13 | Materials

[1,1′-Biphenyl]-3-yl(6-((3-(2-acetamidoethyl)-2-bromo-1H-indol-5-yl) oxy)hexyl)carbamate (UCM1341) was synthesized according to the procedure described by Spadoni et al. (2018). Cyclohexylcarbamic acid 3′-(aminocarbonyl)-[1,1′-biphenyl]-3-yl ester (URB597, Cat# 546141-08-6), N-acetyl-5-methoxytryptamine (melatonin, Cat# 673447), propidium iodide (PI, Cat# P3566), NMDA (Cat# 454575), LPS extracted from Escherichia coli and serotype O55:B5 (Cat# L6529, molecular weight of 50 to 100 kDa, when treated with SDS and heat) were from Merck Life Science S.r.l., Milan, Italy. Recombinant human IFN-γ was from PeproTech, Cat# 300-02. All media and serum for organotypic cultures were purchased from Gibco (Thermo Fisher Scientific, Inc., Waltham, MA, USA). UCM1341, URB597, melatonin, 1-(2,4-dichlorophenyl)-5-(4-iodophenyl)-4-methyl-N-piperidin-1-ylpyrazole-3-carboxamide (AM251, Cayman Chemical, Ann Arbor, MI, USA, Cat# 71670), [6-iodo-2-methyl-1-[2-(4-morpholinyl)ethyl]-1H-indol-3-yl](4-methoxyphenyl)-methanone (AM630, Tocris Bioscience, Bristol, UK, Cat# 1120), (3-(4-chlorophenyl)-N-(3-methoxyphenyl)-2-propenamide) (SB366791, Tocris Bioscience, Bristol, UK, Cat# 472981-92-3), N-[(2S)-3-[4-[2-(5-methyl-2-phenyl-1,3-oxazol-4-yl) ethoxy]phenyl]-2-[[(Z)-4-oxo-4-[4-(trifluoromethyl)phenyl]but-2-en-2-yl]amino]propyl]propanamide (GW6471, Tocris Bioscience, Bristol, UK, Cat# 4618) and N-[2-[2-(phenylmethyl)-1H-indol-3-yl]ethyl]

acetamide (luzindole, Santa Cruz Biotechnology, Inc., Dallas, TX, USA, Cat# 117946-91-5) were dissolved in dimethyl sulfoxide (DMSO; stock solutions of 25 mM), aliquoted and kept frozen at −20°C. NMDA was dissolved in serum-free medium (SFM; stock solution of 10 mM), LPS in pyrogen-free water and IFN-γ in Dulbecco's phosphate-buffered saline containing 0.1% bovine serum albumin (BSA). Stock solutions were diluted to achieve the desired drug concentration immediately before use. Maximal DMSO concentration was ≤0.1%; this concentration did not affect cell viability in organotypic cultures (Boscia et al., 2006).

For analytical determinations, the standards for AEA (Cat# 90050), OEA (Cat# 90265), PEA (Cat# 90350), and their corresponding deuterated (d4) internal standards AEA-d4 (Cat# 10011178), OEA-d4 (Cat# 9000552) and PEA-d4 (Cat# 10007824) were supplied by Cayman Chemical (Ann Arbor, MI, USA) as stock solutions in ethanol. Reduced glutathione (GSH, Cat# G6529) and GSH disulfide (GSSG, Cat# G6654) were purchased from Sigma-Aldrich S.r.l. (Milan, Italy) as powders. High-performance liquid chromatography (HPLC)-grade acetonitrile (Cat# 1.00030.2500) and formic acid (Cat# 84865.180) were supplied by VWR International (Milan, Italy). [^{3}H]-AEA (specific activity: 60 Ci·mmol−1, Cat# 0626-250), employed as a substrate for in vitro FAAH activity assay, was supplied by American Radiolabeled Chemicals (St. Louis, MO, USA). All other chemicals not mentioned otherwise were from Merck Life Science S.r.l., Milan, Italy.

2.14 | Nomenclature of targets and ligands

Key protein targets and ligands in this article are hyperlinked to corresponding entries in http://www.guidetopharmacology.org and are permanently archived in the Concise Guide to PHARMACOLOGY 2021/22 (Alexander, Christopoulos, et al., 2021; Alexander, Cidlowski, et al., 2021; Alexander, Fabbro, et al., 2021; Alexander, Kelly, et al., 2021; Alexander, Mathie, et al., 2021).

3 | RESULTS

3.1 | Neuroprotective effects of UCM1341 against NMDA-induced excitotoxicity in organotypic hippocampal explants

To study the neuroprotective potential of the bivalent ligand UCM1341, we investigated the effects of 0.1–10 μM UCM1341 against a milder and more severe excitotoxic insult induced by 10 or 30 μM NMDA exposure (Boscia et al., 2006). When hippocampal explants were exposed to 10 μM NMDA for 48 h, cell death selectively occurred in the CA1 pyramidal cell layer and, to a lesser degree, in the CA3. By contrast, higher concentrations of 30 μM NMDA caused more marked neurodegenerative effects that involved both CA1 and CA3 (Figure 1). When slices were incubated with 10 μM NMDA, a significant prevention of PI uptake in the CA1 region was observed with 1–10 μM UCM1341 (about 30%) (Figure 1a–c). Conversely, the bivalent ligand was less effective in counteracting CA degeneration induced by 30 μM NMDA, and a significant neuroprotective effect was observed only with 10 μM UCM1341 (Figure 1d–f).

Then, we investigated the synergistic neuroprotective potential of reference compounds, melatonin and URB597, against NMDA-induced neurodegeneration. To this aim, hippocampal explants were exposed to 10 μM NMDA, in the absence or presence of melatonin or URB597, alone or in combination. As shown in Figure 1g, 10 μM melatonin, but not 10 μM URB597, exerted a significant neuroprotection in the CA1 against NMDA-induced excitotoxicity (about 35%). When melatonin and URB597 were applied in combination (both at 10 μM), a significant neuroprotection was observed in the CA1 region, an effect that was comparable to that of melatonin and was not statistically different from that of UCM1341 (Figure 1g–i). Drug treatments in control slices did not affect cell viability at any of the concentrations used or time points analysed, as revealed by PI uptake.

3.2 | LPS + IFN-γ exposure preferentially induced inflammatory degeneration in the CA1 region and modulated FAAH enzyme and melatonin receptor expression in brain cells

Next, to study the neuroprotective potential of UCM1341 on neuroinflammatory damage, hippocampal slice cultures were exposed to a combined application of 10 μg·ml^{-1} LPS and 100 ng·ml^{-1} recombinant IFN-γ for 3–4 days. We show that the cell degeneration, which abruptly appeared after 72 h (in 7 DIV slices) or 96 h (in 10 DIV slices) of LPS + IFN-γ exposure, can be monitored by PI uptake in hippocampal explant cultures (Figure 2a–d). Quantitative densitometric analysis showed that when the insult was applied to hippocampal slice cultures at 7 DIV, a significant up-regulation of PI uptake in the CA1 region was recorded after 72 h, whereas the CA3 and dentate gyrus (DG) subregions were less affected (Figure 2a,b). When 10 DIV hippocampal cultures were exposed to LPS + IFN-γ, PI uptake significantly and selectively increased in the CA1 region after 96 h (Figure 2c,d). The pro-inflammatory insult significantly up-regulated the protein levels of the microglial Iba1 marker after 48 h of LPS + IFN-γ exposure (Figure 2e,f) and induced demyelination, as revealed by the significant reduction of MBP levels (Figure 2i,j) and MBP immunoreactivity after 72 h (Figure 2m). Next, we investigated the effects of the inflammatory insult on the expression of the endocannabinoid hydrolysing enzyme FAAH and of melatonin receptors. As shown in Figure 2g,h, FAAH levels transiently increased at 24 h, whereas the non-selective anti-MT$_1$/MT$_2$ receptor antibody revealed that both MT$_1$ and MT$_2$ levels concomitantly and transiently increased 48 h after the insult (Figure 2i,k,l). In line with previous studies (Gulyas et al., 2004), confocal analysis performed with anti-FAAH antibodies in hippocampal explants showed the predominant distribution of FAAH enzyme in somata and dendrites of principal cells (Figure 3a–c). Quantitative confocal analysis in the CA1 region revealed that the fluorescence intensity of both FAAH and GFAP, but not of MAP2 and
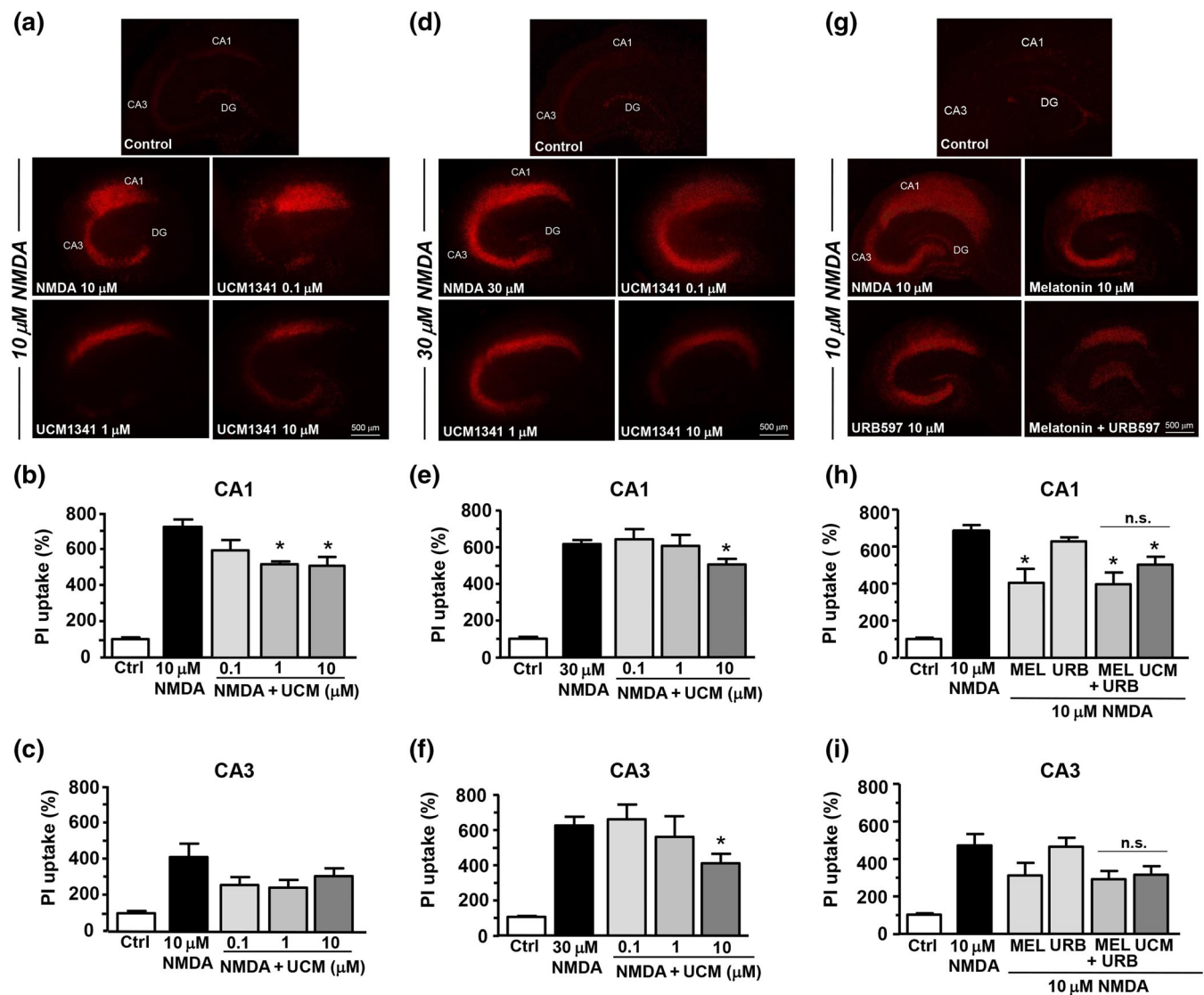
FIGURE 1 Dose-dependent effects of UCM1341 against N-methyl-D-aspartate (NMDA)-induced neurodegeneration in hippocampal explants. Propidium iodide (PI) fluorescence staining patterns (a) and densitometric quantification of PI uptake in hippocampal CA1 (b) and CA3 (c) subfields measured under control conditions and following 10 μM NMDA exposure in the absence or presence of 0.1–10 μM UCM1341 for 48 h. PI fluorescence staining patterns (d) and densitometric quantification of PI uptake in hippocampal CA1 (e) and CA3 (f) subfields measured under control conditions and following 30 μM NMDA exposure in the absence or presence of 0.1–10 μM UCM1341 for 48 h. PI fluorescence staining patterns (g) and densitometric quantification of PI uptake in hippocampal CA1 (h) and CA3 (i) subfields measured under control conditions and following 10 μM NMDA exposure in the absence or presence of 10 μM melatonin, 10 μM URB597 or 10 μM melatonin + 10 μM URB597. Data are normalized as percentage of control and are means ± SEM; n = 5. *$P < 0.05$, significantly different from NMDA; n.s., not significant; one-way ANOVA with Bonferroni post hoc analysis.

the microglial marker CD11b, significantly increased 24 h after LPS + IFN-γ exposure, compared with values in untreated controls (Figure 3a,b,e). At this latter time point, co-expression studies showed a significant increase of FAAH expression in MAP2$^+$ neurons and GFAP$^+$ astrocytes (Figure 3a,b,f). After 48 h, FAAH immunofluorescence returned to basal level, whereas GFAP and CD11b immunofluorescences were significantly up-regulated (Figure 3c,d,g). Nevertheless, quantitative confocal analysis revealed a significant increased co-expression of FAAH with CD11b$^+$ microglia and GFAP$^+$ astrocytes, but not with MAP2$^+$ neurons (Figures 3c,d,h and S1).

3.3 | UCM1341 attenuated LPS + IFN-γ-induced demyelination and GABAergic interneuron loss and exerted a greater neuroprotection against the neuroinflammatory insult, compared with effects of the reference compounds melatonin and URB597

To investigate the effects of UCM1341 on inflammation-mediated neurodegeneration, 10 DIV slices were exposed to 10 μg·ml^{-1} LPS + 100 ng·ml^{-1} IFN-γ, in the absence or presence of 0.1–10 μM UCM1341 for 4 days. Densitometric analysis of PI uptake revealed that
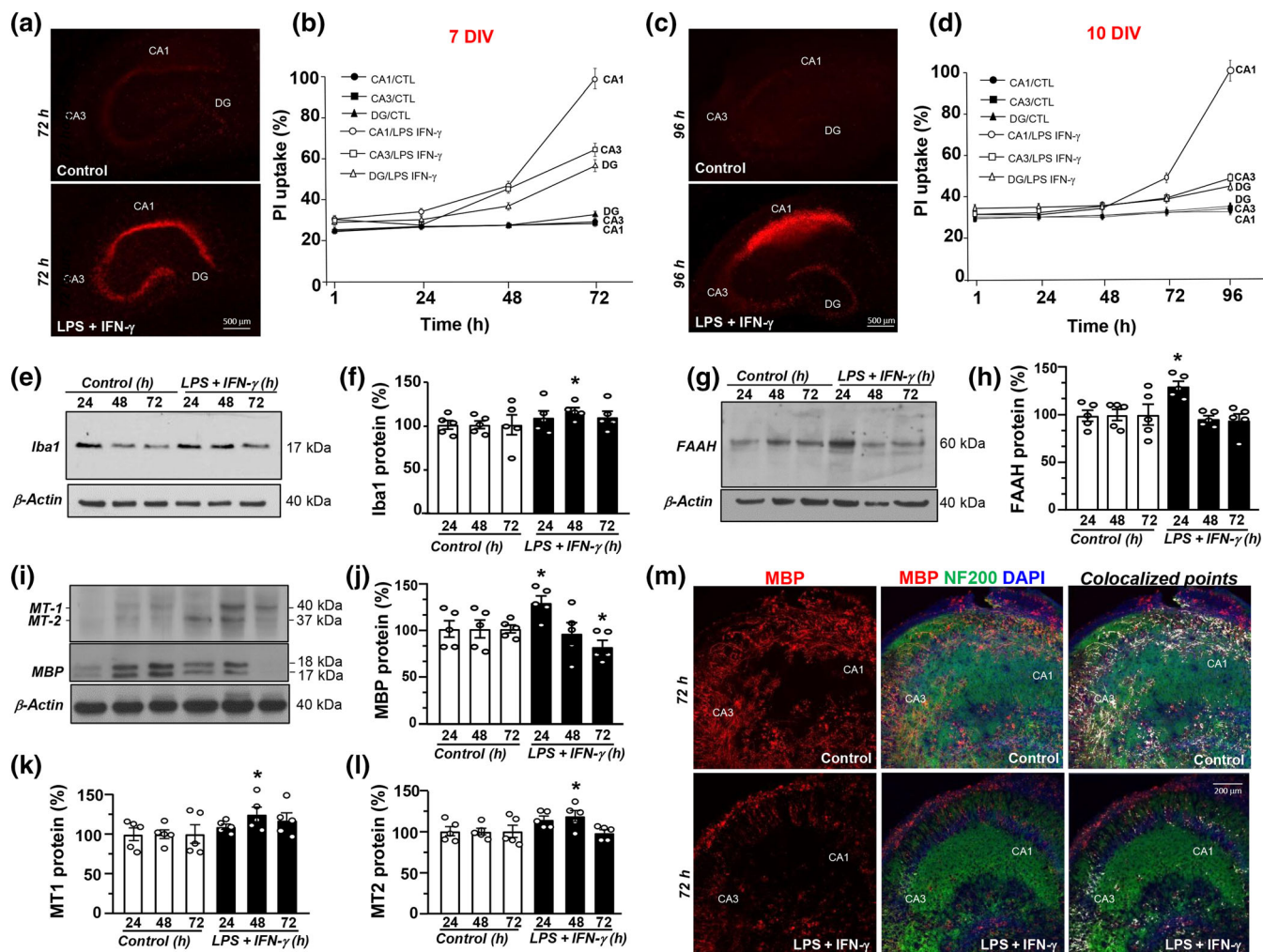
FIGURE 2 Time-dependent effects of lipopolysaccharide (LPS) + interferon-γ (IFN-γ) exposure on propidium iodide (PI) uptake, and Iba1, myelin basic protein (MBP), fatty acid amide hydrolase (FAAH) and melatonin receptor protein levels in rat hippocampal explants. Representative images and quantitative densitometric analysis of PI fluorescence uptake recorded in the cornu ammonis (CA) and dentate gyrus (DG) subfields of 7 days in vitro (DIV) slices (a, b) or 10 DIV slices (c, d) exposed to LPS + IFN-γ for 72 or 96 h, respectively. Data are expressed as percentage of the maximal value of PI fluorescence observed in the CA1 subregion upon 72 or 96 h of LPS + IFN-γ exposure, respectively. Each data point is the mean ± SEM (n = 5). Western blot and quantification of Iba1 (e, f), FAAH (g, h), melatonin MT_1/MT_2 receptors (i, k, l) and MBP (i, j) protein levels in hippocampal slices under control conditions and after LPS + IFN-γ exposure for 24–72 h. Data were normalized on the basis of β-actin and expressed as percentage of controls. The values shown are the means ± SEM; n = 5. *$P < 0.05$, significantly different from respective controls; one-way ANOVA with Bonferroni post hoc analysis. (m) Representative confocal double immunofluorescence images displaying the distribution of MBP (red) and NF200 (green) immunoreactivities and their co-localization (white) in untreated and LPS + IFN-γ-treated slices for 72 h.

UCM1341 exerted marked and dose-dependent neuroprotective actions in the more vulnerable CA1 region. At 10 μM, UCM1341 decreased cell death occurring after LPS + IFN-γ exposure (Figure 4a,b).

To explore the synergistic neuroprotective potential of reference compounds, hippocampal explants were exposed to LPS + IFN-γ in the absence or presence of 10 μM melatonin or 10 μM URB597, alone or in combination. Both melatonin and URB597 exerted a significant neuroprotection against LPS + IFN-γ-induced neurodegeneration (about 30%), as recorded by PI uptake after 96 h. When drugs were used in combination (both at 10 μM), they completely prevented cell death in the CA1 region, thus demonstrating the synergistic neuroprotective effect of melatonin and URB597 against LPS + IFN-γ-

induced inflammatory damage (Figure 4c,d). The neuroprotective effect of combined drugs (each at 10 μM) was not statistically different from that of 10 μM UCM1341.

Next, to explore the protective effects of UCM1341 on myelin and neurons during LPS + IFN-γ exposure, hippocampal explants were analysed for MBP/NF200 co-localization and GABA distribution by confocal analysis. UCM1341 significantly prevented the loss of NF200 immunoreactivity (Figure 4e,f) and inhibitory GABA+ interneurons in the CA1 region (Figure 4h,i). Moreover, treatment with UCM1341 attenuated axonal demyelination induced by LPS + IFN-γ exposure, as indicated by the quantification of the myelination index 96 h after the insult (Figure 4g).
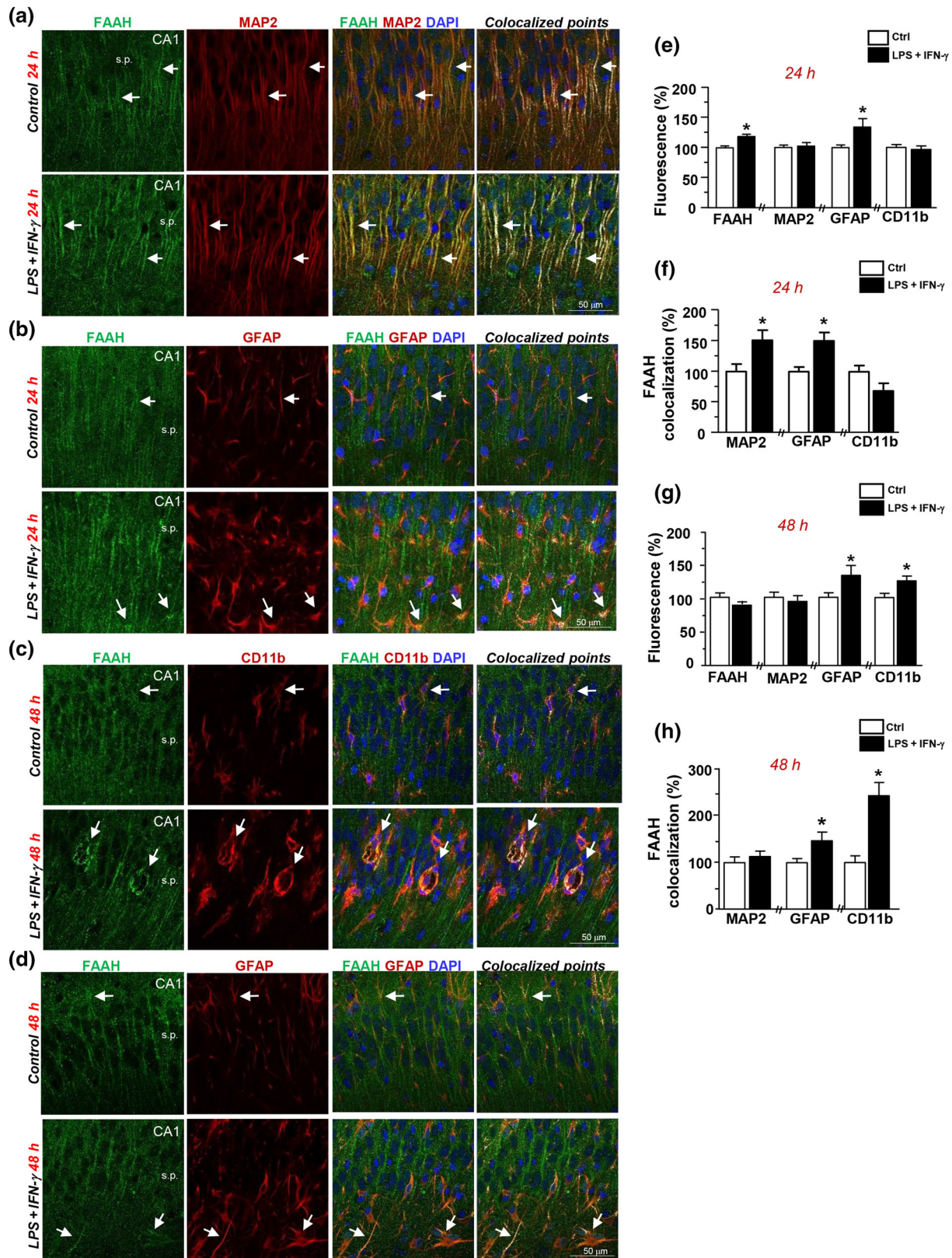
FIGURE 3 Legend on next page.

3.4 | UCM1341 inhibited FAAH activity and enhanced AEA and OEA in hippocampal explants during the neuroinflammatory injury

To investigate the mechanism of UCM1341 in counteracting inflammation-mediated neurodegeneration, FAAH activity was evaluated after drug exposure to a concentration of 10 μM. FAAH remained completely inhibited at all time points (24–72 h, Figure 5a). The levels of FAAH substrates AEA, OEA and PEA were also measured in the same conditions. Although treatment with $10\ \mu g \cdot ml^{-1}$ LPS + $100\ ng \cdot ml^{-1}$ IFN-γ did not alter the concentrations of the three *N*-acylethanolamines, UCM1341 produced a significant increase of AEA and OEA concentrations at all time points, in line with the persistent inhibition of FAAH activity (Figure 5b,c). On the other hand, PEA levels were not affected by UCM1341 and remained at concentrations comparable to those of untreated samples (Figure 5d). We next evaluated the changes in GSH and GSSG levels, as markers of cell oxidative stress. Ten DIV slices exposed to LPS + IFN-γ showed a trend to reduction of GSH availability at all time points. Treatment with UCM1341 did not alter GSH levels or the GSH/GSSG ratio (Figure 5e,f).

3.5 | UCM1341 prevented TNFα release, up-regulated the expression of the anti-inflammatory markers CD206 and arginase-1, and increased AMPK phosphorylation in hippocampal explants

To address the effects of drug treatment on inflammatory response, we analysed the expression of pro-inflammatory cytokines as well as markers of anti-inflammatory pathways. Quantitative ELISA analysis showed that LPS + IFN-γ exposure for 24–72 h progressively increased the release of pro-inflammatory (IL-6) and anti-inflammatory (IL-10) cytokines (Figure 6a,b). Interestingly, although the levels of IL-6 and IL-10 were not affected by drug treatment (Figure 6a,b), UCM1341 prevented the release of TNFα, in both the medium and tissue lysates after 72 h (Figure 6c). Immunoblotting revealed that the protein levels of the M2 macrophage markers, the mannose receptor CD206 and Arg-1, were significantly higher in UCM1341-treated slices after 72 h of LPS + IFN-γ exposure, compared with untreated and LPS + IFN-γ-treated slices (Figure 6d,g). Consistent with these

findings, UCM1341 treatment increased the number of CD206+ cells, suggesting an effect of UCM1341 on microglial polarization (Figure 6e,f).

Recently, activation of AMPK, a serine/threonine kinase regulating cellular energy homeostasis, has emerged as a negative regulator of inflammation and a 'metabolic master switch' of macrophage polarization (Trefts & Shaw, 2021). Based on these observations, we hypothesized that the inflammation suppressive effects of UCM1341 might involve AMPK activation. Immunoblot showed that 10 μM UCM1341 treatment for 72 h significantly increased phospho-AMPK levels, compared with those in LPS + IFN-γ-treated explants (Figure 6h).

3.6 | UCM1341 stimulated the formation of lipid-laden foamy microglia/macrophages and cholesterol homeostasis during LPS + IFN-γ-induced neuroinflammation

UCM1341 prevented the loss of microglia and astrocytes in the CA1 pyramidal layer, 96 h after the inflammatory injury, as revealed by the significantly higher number of Iba1+ cells and GFAP+ area measured in the CA1 region compared with untreated cultures (Figure 7a–c). Morphological assessment of Iba1+ cells showed that dystrophic microglia dominate the CA1 pyramidal layer of LPS + IFN-γ-exposed explants after 96 h, whereas the foamy microglia/macrophage phenotype was clearly prevalent in slices treated with 10 μM UCM1341 during the inflammatory insult (Figure 7d,e).

Recent evidence has indicated that the expression of nuclear and plasma membrane receptors coupling lipid metabolism to efficient cholesterol recycling in foamy macrophages is important for an efficient phagocytosis and cholesterol efflux in response to demyelination and, consequently, for resolution of inflammation and remyelination in the CNS (Gouna et al., 2021). Thus, we explored the effect of UCM1341 treatment on lipid-laden macrophage formation and the expression of protein regulating cholesterol metabolism and efflux. UCM1341 treatment up-regulated the protein levels of TREM2 (Figure 8a), a lipid sensor receptor that licenses phagocytosis (Gouna et al., 2021), the cholesterol-sensing nuclear receptor LXR and the cholesterol efflux transporter ABCA1 (Figure 8b), compared with untreated and LPS + IFN-γ-treated slices for 72 h. Also, quantitative

---

FIGURE 3 Distribution of fatty acid amide hydrolase (FAAH) immunoreactivity in neurons, astrocytes and microglia of hippocampal explants during lipopolysaccharide (LPS) + interferon-γ (IFN-γ) exposure. Representative confocal images displaying the co-localization of FAAH with microtubule-associated protein 2 (MAP2) (a) or FAAH with glial fibrillary acidic protein (GFAP) (b) immunoreactivities in the CA1 hippocampal region, in the absence or presence of LPS + IFN-γ for 24 h. Confocal images displaying co-localization of FAAH with CD11b (c) or FAAH with GFAP (d) immunoreactivities in the CA1 hippocampal region, in the absence or presence of LPS + IFN-γ for 48 h. In (a)–(d), co-localized points are shown in white. Arrows in (a) point to co-localizing dendrites. Arrows in (b)–(d) point to co-localizing cells. Quantitative analysis of FAAH, MAP2, GFAP and CD11b immunofluorescence intensities (e) and FAAH co-localization with MAP2, GFAP or CD11b immune-signals (f) in the CA1 hippocampal region, in the absence or presence of LPS + IFN-γ for 24 h. Quantitative analysis of FAAH, MAP2, GFAP and CD11b immunofluorescence intensities (g) and FAAH co-localization with MAP2, GFAP and CD11b immune-signals (h) in the absence or presence of LPS + IFN-γ for 48 h. Data were obtained from five microscope fields per slice in each group and expressed as percentage of control. The values shown are the means ± SEM; n = 5. *$P < 0.05$, significantly different from respective control; unpaired Student's t test. s.p., stratum pyramidale.
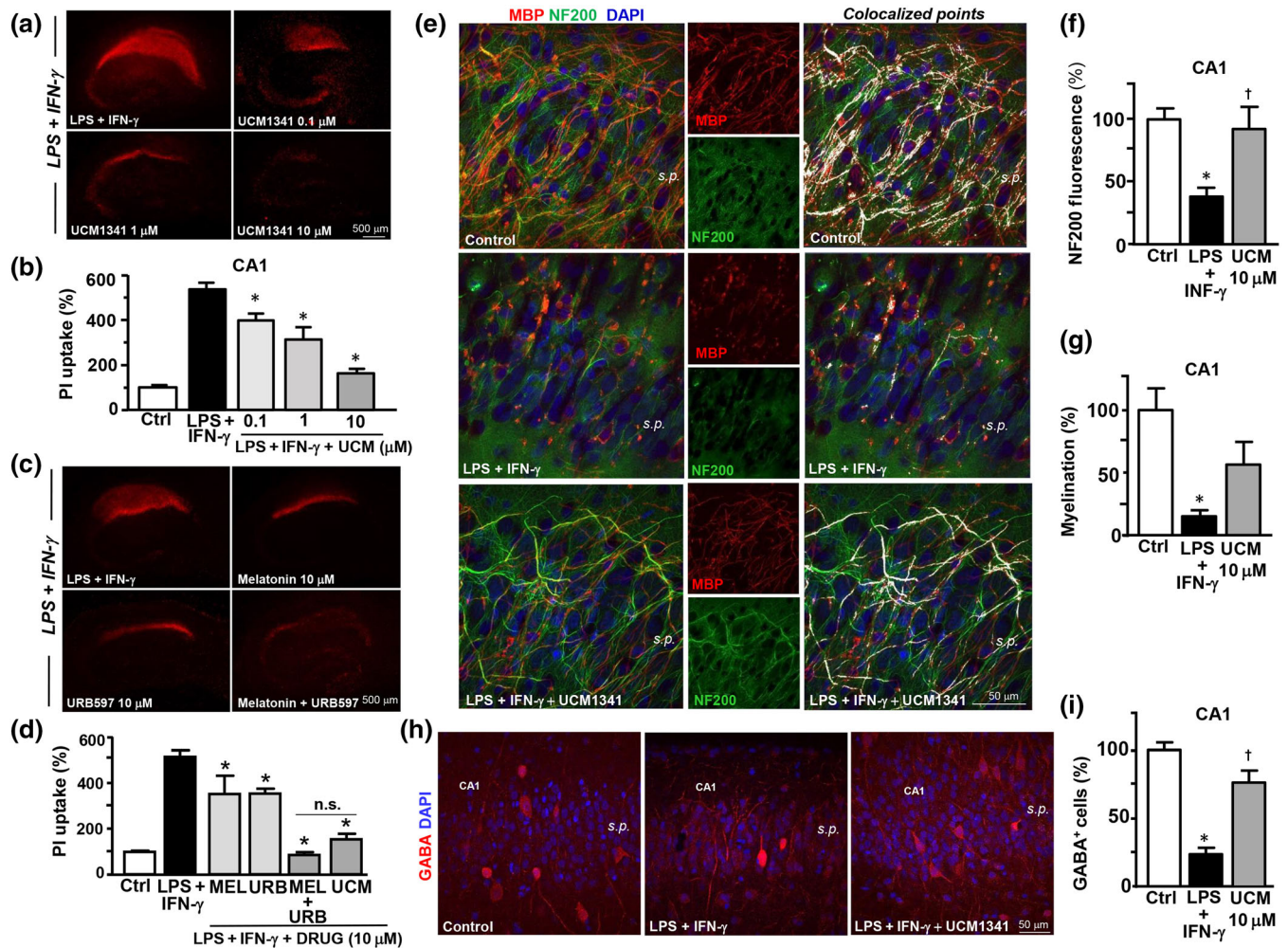
FIGURE 4 Protective effects of UCM1341 against neuroinflammation-induced degeneration. Propidium iodide (PI) fluorescence staining patterns (a) and quantitative densitometric analysis of PI uptake (b) in the CA1 region following lipopolysaccharide (LPS) + interferon-γ (IFN-γ) exposure in the absence or presence of 0.1–10 μM UCM1341 for 96 h. The values shown are the means ± SEM; n = 5. *P < 0.05, significantly different from LPS + IFN-γ; one-way ANOVA with Bonferroni post hoc analysis. PI fluorescence staining patterns (c) and quantitative densitometric analysis of PI uptake (d) in the CA1 region following LPS + IFN-γ exposure in the absence or presence of 10 μM melatonin, 10 μM URB597, 10 μM melatonin + 10 μM URB597 and 10 μM UCM1341 for 96 h. The values shown are the means ± SEM; n = 5. *P < 0.05, significantly different from LPS+IFN-γ; n.s., not significant; one-way ANOVA with Bonferroni post hoc analysis. (e) Representative maximum intensity projection of z-stack confocal images displaying NF200 (green) and myelin basic protein (MBP) (red) immunoreactivities in the CA1 region of 10 days in vitro (DIV) hippocampal slices under control conditions and LPS + IFN-γ exposure, in the absence or presence of 10 μM UCM1341 for 96 h. Colocalized points are shown in white. (f) Quantitative analysis of NF200 immunofluorescence intensity under control conditions and in the presence of LPS + IFN-γ and LPS + IFN-γ + 10 μM UCM1341. The values shown are the means ± SEM; n = 5. *P < 0.05, significantly different from control; †P < 0.05, significantly different from LPS + IFN-γ; one-way ANOVA with Bonferroni post hoc analysis. (g) Analysis of the myelination index in the pyramidal/oriens layers of the CA1 region in 10 DIV hippocampal slices under control conditions and following LPS + IFN-γ exposure in the absence or presence of UCM1341. The values shown are the means ± SEM; n = 5. *P < 0.05, significantly different from control; one-way ANOVA with Bonferroni post hoc analysis. (h) Representative confocal images and quantitative analysis (i) of GABA-positive cells in the pyramidal layer of the CA1 hippocampal region, under control conditions or following LPS + IFN-γ in the absence or presence of 10 μM UCM1341 for 96 h. The values shown are the means ± SEM; n = 5. *P < 0.05, significantly different from control. †P < 0.05, significantly different from LPS + IFN-γ; one-way ANOVA with Bonferroni post hoc analysis. s.p., stratum pyramidale.

confocal analysis in the CA1 pyramidal layer showed an increased number of Iba1+ cells coexpressing both the lipid droplet marker Plin2 (Figure 8c,d) and the cholesterol transporter ABCA1 in UCM1341-treated explants under neuroinflammatory conditions (Figure 8e,f).

Finally, to explore whether the formation of lipid-laden microglia/macrophages might also be influenced by the reference compounds, we investigated the effects of melatonin and URB597 (10 μM), alone or in combination, on the number of Iba1+/Plin2+ cells after LPS + IFN-γ exposure for 72 h. Quantitative confocal analysis revealed
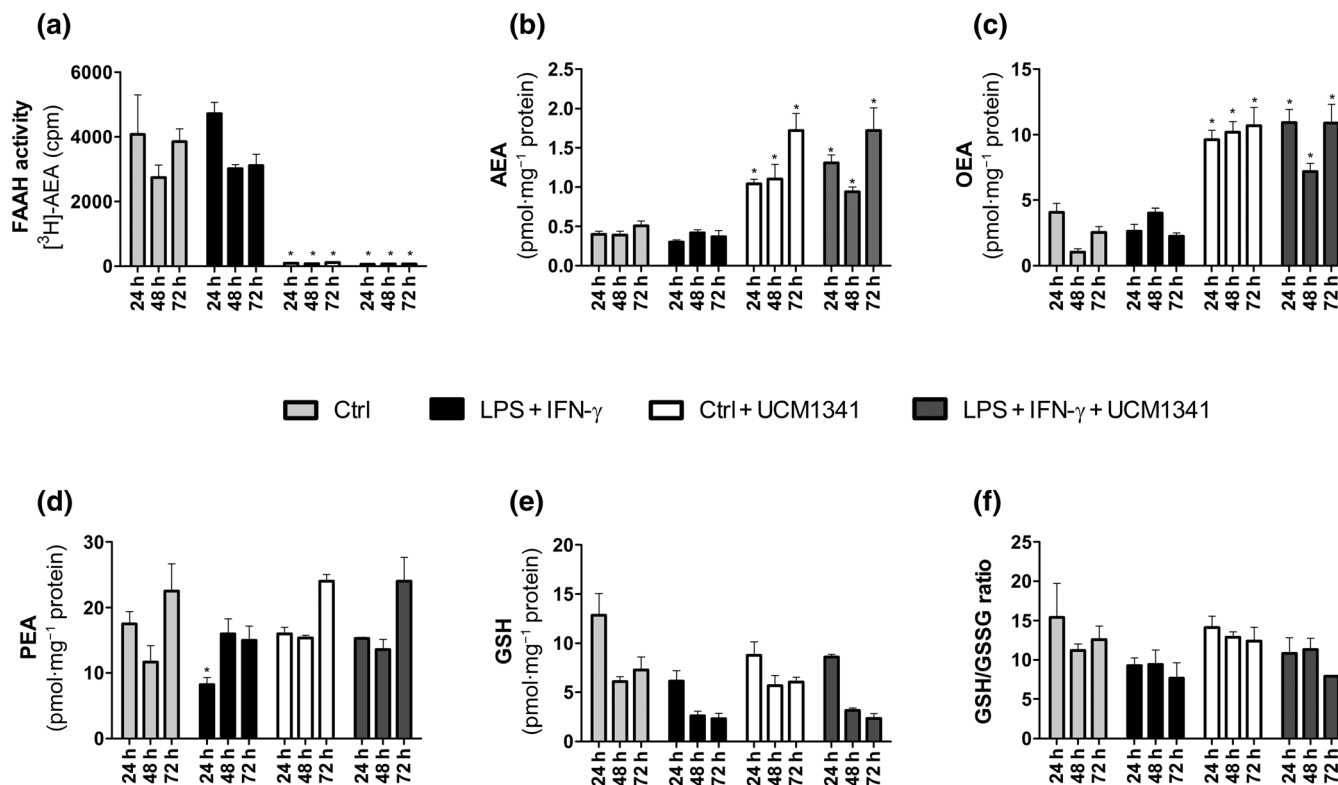
FIGURE 5 Effect of UCM1341 on fatty acid amide hydrolase (FAAH) activity and glutathione (GSH) levels in hippocampal cultures. FAAH activity (a), anandamide (AEA, b), N-oleoylethanolamine (OEA, c), N-palmitoylethanolamine (PEA, d), reduced GSH (e) levels and (f) GSH/GSH disulfide (GSSG) ratios in organotypic hippocampal slices under control conditions or after lipopolysaccharide (LPS) + interferon-γ (IFN-γ) exposure in the absence or presence of 10 μM UCM1341 for 24–72 h (Ctrl), LPS + IFN-γ, Ctrl + 10 μM UCM1341 and LPS + IFN-γ + 10 μM UCM1341. The values shown are the means ± SEM; n = 5. *$P < 0.05$, significantly different from respective control; one-way ANOVA with Bonferroni post hoc analysis.

that the number of Iba1+/Plin2+ cells was significantly higher in cultures treated with LPS + IFN-γ + melatonin+ URB597 compared with untreated slices or slices treated with LPS + IFN-γ, in the absence or presence of melatonin or URB597 (Figure 8g,h). These results suggest a synergistic action of melatonin and URB597 on the formation of foamy macrophages.

3.7 | PPARα, TRPV1 channels and MT$_1$/MT$_2$ receptors all significantly contributed to the neuroprotective effect of UCM1341

To investigate the role of endocannabinoid and melatonin receptors on UCM1341 protective effects against LPS + IFN-γ-induced neuroinflammation in hippocampal explants, we examined the possible interference of specific antagonists of CB$_1$ and CB$_2$ receptors, TRPV1 channels, melatonin receptors and PPARα. Antagonists were used at concentrations that displayed no effect when used alone. As shown in Figure 9a,b, quantitative densitometric analysis of PI uptake revealed that the neuroprotective effect of 10 μM UCM1341 in the CA1 region was significantly prevented by antagonists of PPARα (10 μM GW6471), TRPV1 channels (30 nM SB366791) and melatonin

receptors (0.1 μM luzindole). Conversely, both the CB$_1$ and CB$_2$ antagonists, that is, 0.1 μM AM251 and 0.1 μM AM630, failed to antagonize UCM1341-induced neuroprotection in LPS + IFN-γ-treated cultures. Finally, to investigate the possible cross-talk of the endocannabinoid and melatoninergic systems, we explored the expression of PPARα protein levels early after the inflammatory insult, in the absence or presence of UCM1341 or reference compounds. As shown in Figure 9c, 10 μM UCM1341 and combined 10 μM URB597 + 10 μM melatonin significantly increased the expression of PPARα levels after 8 h of LPS + IFN-γ exposure, compared with untreated controls. No significant difference was found between 10 μM UCM1341 and URB597 + melatonin (each at 10 μM). These findings suggest that a cross-talk between the endocannabinoid and melatoninergic pathways via the activation of PPARα may contribute to the beneficial effects of the bivalent ligand.

4 | DISCUSSION

The present study shows that the newly synthesized compound UCM1341, a bivalent ligand exhibiting FAAH inhibitory activity and melatonin receptor agonism, exerts a greater neuroprotection against
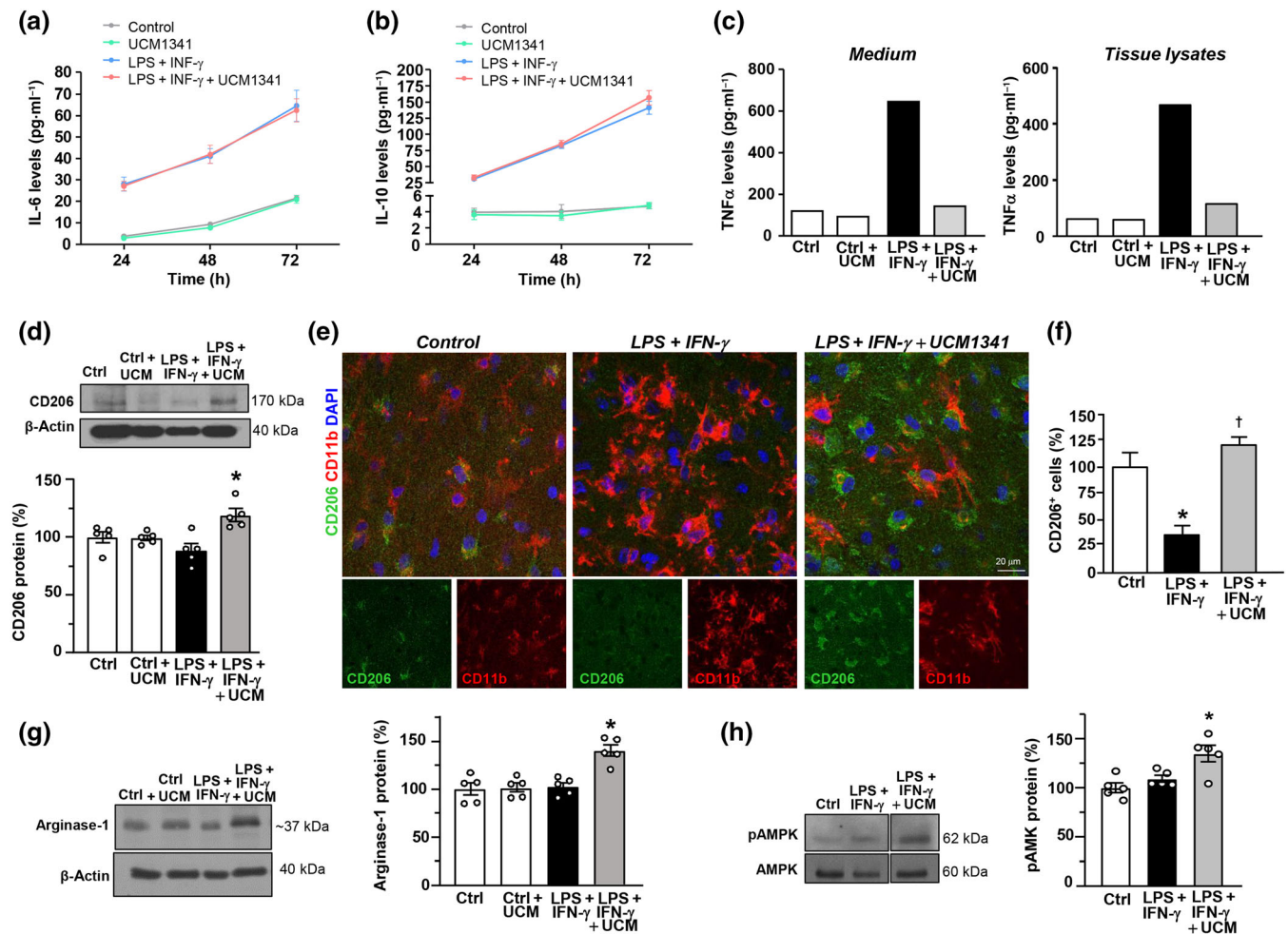
FIGURE 6 Effect of UCM1341 on IL-6 and IL-10 production, TNFα release, CD206 and Arg-1 levels, and AMPK phosphorylation. Time-dependent production of IL-6 (a) and IL-10 (b) in the medium of explants cultures under control conditions or lipopolysaccharide (LPS) + interferon-γ (IFN-γ) exposure in the absence or presence of 10 μM UCM1341 for 24–72 h. The values shown are the means ± SEM; n = 3. (c) TNFα determination in the medium (left) and tissue lysates (right) of hippocampal cultures under control conditions, and LPS + IFN-γ exposure in the absence or presence of 10 μM UCM1341 for 72 h. Experiments were performed in duplicate. (d) Western blot and densitometric analysis of CD206 protein levels in hippocampal lysates under control conditions and after LPS + IFN-γ exposure in the absence or presence of 10 μM UCM1341 for 72 h. Data were normalized on the basis of β-actin levels and expressed as percentage of control. The values shown are the means ± SEM; n = 5. *$P < 0.05$, significantly different from LPS + IFN-γ; one-way ANOVA with Bonferroni post hoc analysis. (e) Representative confocal microscopic images showing CD206 and CD11b immunoreactivities in the CA1 hippocampal region under control conditions, LPS + IFN-γ exposure and LPS + IFN-γ + 10 μM UCM1341. (f) Quantitative analysis of CD206+ cells in slices under control conditions, LPS + IFN-γ and LPS + IFN-γ + 10 μM UCM1341 exposure for 72 h. Data are expressed as percentage of control. The values shown are the means ± SEM; n = 5. *$P < 0.05$, significantly different from control, †$P < 0.05$, significantly different from LPS + IFN-γ; one-way ANOVA with Bonferroni post hoc analysis. (g) Western blot and densitometric analysis of arginase-1 in hippocampal slices under control conditions and LPS + IFN-γ exposure in the absence or presence of 10 μM UCM1341 for 72 h. The values represent the mean ± SEM (n = 5). *$P < 0.05$, significantly different from control and LPS + IFN-γ; one-way ANOVA with Bonferroni post hoc analysis. (h) Western blot and densitometric analysis of pAMPK levels in hippocampal slices under control conditions and LPS + IFN-γ exposure in the presence of 10 μM UCM1341 for 72 h. Data were normalized on the basis of AMPK levels and expressed as percentage of control. The values shown are the means ± SEM; n = 5. *$P < 0.05$, significantly different from control and LPS + IFN-γ; one-way ANOVA with Bonferroni post hoc analysis.

neuroinflammation-induced degeneration in hippocampal explants than the reference compounds, URB597 and melatonin, and encourages inflammation resolution contributing to the formation of lipid-laden macrophages and the expression of proteins controlling cholesterol metabolism and efflux. The activation of PPARα, TRPV1 channels and melatonin receptors and a cross-talk between the endocannabinoid and melatoninergic systems contribute to the

beneficial effects of UCM1341 during the neuroinflammatory insult. We showed that the neurodegeneration occurring in the CA1 hippocampal region after exposure of explants to LPS + IFN-γ, a model of inflammatory degeneration, can be monitored by PI uptake. This model of damage replicates the main markers of inflammatory demyelinating CNS diseases, including glial activation, axonal demyelination and neuronal loss (Boscia et al., 2020, 2021), and can be used to study
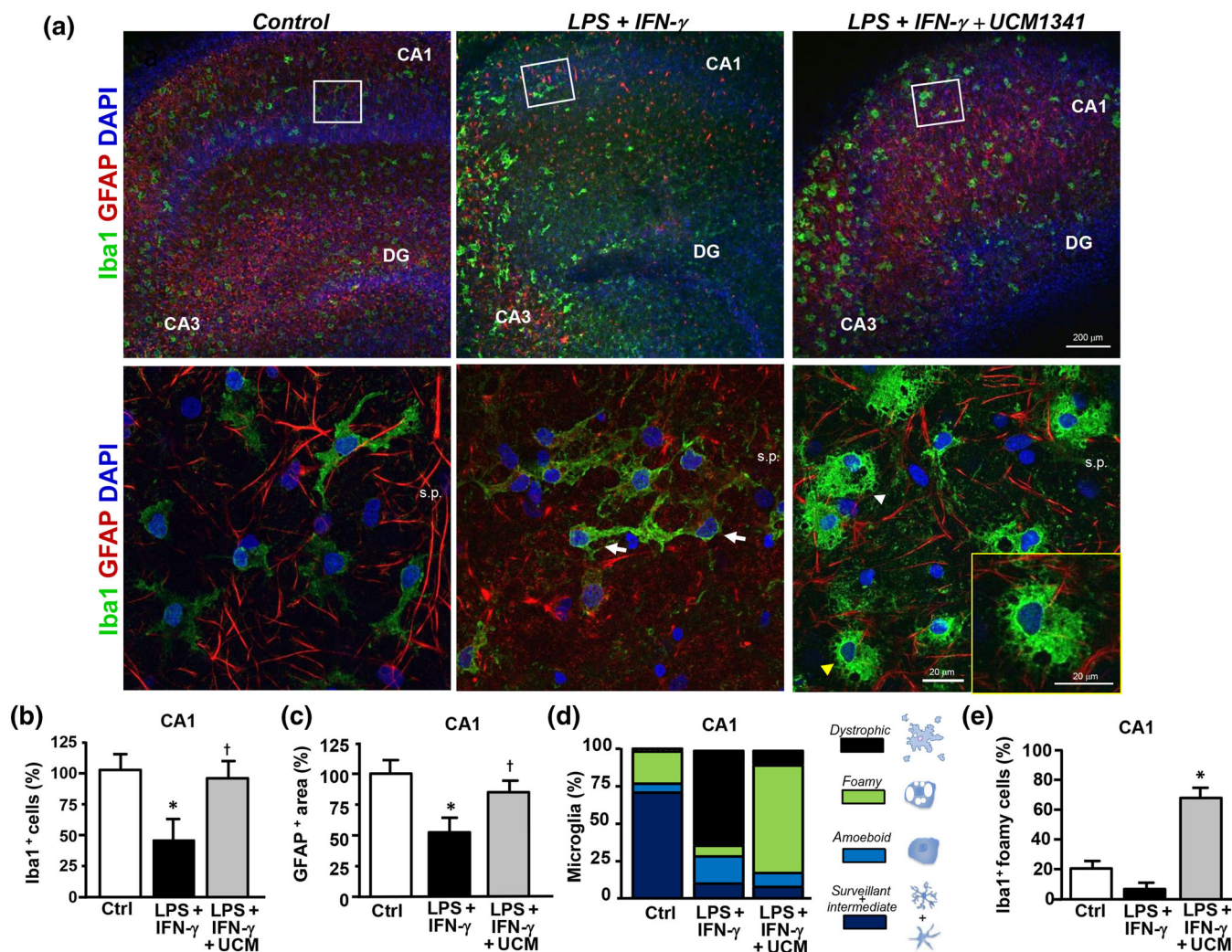
FIGURE 7 Effect of UCM1341 on microglia and astrocyte immunoreactivities following lipopolysaccharide (LPS) + interferon-γ (IFN-γ) exposure. (a) Representative confocal microscopic images showing Iba1 (green) and glial fibrillary acidic protein (GFAP) (red) immunoreactivities in the stratum pyramidale (s.p.) of the CA1 hippocampal region of cultures under control conditions and after LPS + IFN-γ exposure in the absence or presence of 10 μM UCM1341 for 96 h. Lower panels show higher magnification images of squared areas. Arrows point to atrophic microglia. Arrowheads point to foamy microglia/macrophages. The yellow arrowhead points to a foamy macrophage that is showed at higher magnification in the lateral box. Quantitative analysis of Iba1$^+$ cells (b) and GFAP$^+$ area (c) in control and LPS + IFN-γ-treated cultures, in the absence or presence of 10 μM UCM1341. The values shown are the means ± SEM; n = 5. *$P < 0.05$, significantly different from control; $^\dagger P < 0.05$, significantly different from LPS + IFN-γ; one-way ANOVA with Bonferroni post hoc analysis. (d) Quantitative analysis of surveillant + intermediate, amoeboid, foamy and dystrophic microglial phenotypes, in control and LPS + IFN-γ-treated cultures, in the absence or presence of 10 μM UCM1341. Data were normalized to the total number of Iba$^+$ cells. The schematic diagram of microglial phenotypes is shown next to the graph. (e) Quantitative analysis of foamy microglia/macrophages in control and LPS + IFN-γ-treated cultures, in the absence or presence of 10 μM UCM1341. The values shown are the means ± SEM; n = 5. *$P < 0.05$, significantly different from control and LPS + IFN-γ; one-way ANOVA with Bonferroni post hoc analysis.

the effects of pharmacological agents against the neuroinflammatory damage.

Dysregulation of the levels of endocannabinoids, melatonin release and alteration of melatonin receptor expression can be found in many chronic inflammatory conditions of the CNS and contribute to cell dysfunction and disease progression (Chiurchiù et al., 2018; Reiter et al., 2013). We showed that FAAH levels increased in hippocampal CA1 pyramidal neurons and astrocytes, soon after the neuroinflammatory insult and also emerged in microglia at later time

points. Consistent with these findings, FAAH mRNA and protein levels were increased in astrocytes at asymptomatic and acute experimental autoimmune encephalomyelitis (EAE) stage and in glial cells surrounding Aβ plaques in AD and Down syndrome brain tissue (Benito et al., 2003, 2007; Moreno-García et al., 2020; Núñez et al., 2008). Under neuroinflammatory conditions, the enhanced FAAH expression and activity contribute to the 'sickness behaviour', a core symptom of mood disorders. Stress-related disorders and nerve injury also up-regulate FAAH levels, contributing to the dis-inhibition
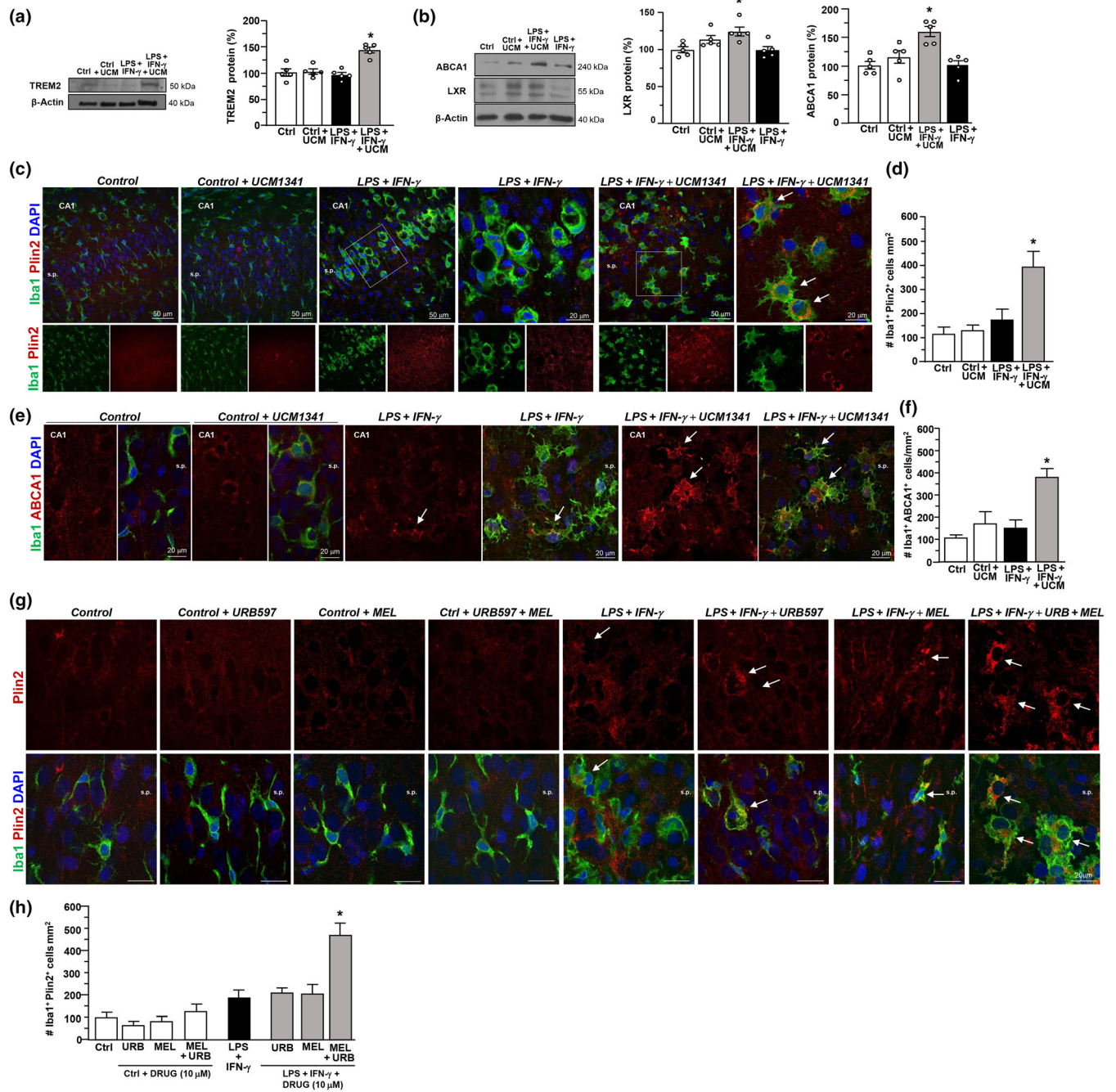
FIGURE 8 Legend on next page.

of the hypothalamic–pituitary–adrenal axis and the development of chronic pain, respectively (Piomelli & Mabou Tagne, 2022).

Conversely, melatonin deficiency and a decline of melatonin receptor levels have been described in Parkinson's disease, AD and amyotrophic lateral sclerosis brains (Adi et al., 2010; Savaskan et al., 2005; Zhang et al., 2013). Interestingly, in AD brain, MT_1 density increased in hippocampal pyramidal neurons, whereas MT_2 levels decreased (Savaskan et al., 2002). Our biochemical studies showed a transient increase of melatonin receptor levels following LPS + IFN-γ exposure and a tendency for MT_2 protein to decline at later times. To what extent changes in melatonin receptor levels are associated with signalling differences in neurons and glia under neuroinflammatory conditions remains to be investigated.

Our studies showed that UCM1341 exerted a greater neuroprotection against the neuroinflammatory damage than against the NMDA insult, and attenuated axonal demyelination and GABAergic loss. In support of the greater benefit provided by FAAH inhibition to the inflammatory component of damage, previous studies showed that URB597 significantly attenuated excitotoxic neurodegeneration when only a mild insult was applied (Mikheeva et al., 2017). This latter observation may support our results showing the predominant contribution of the melatoninergic component to the protective action of UCM1341 under excitotoxic conditions. In fact, melatonin was effective as UCM1341 against NMDA-induced neurodegeneration, and no synergistic neuroprotective action was observed with combined melatonin+ URB597, indicating that dual-acting compounds do not appear a promising approach in the case of excitotoxic damage. The protective effects of endocannabinoids and melatonin have been largely documented in a range of pathological states, particularly in disorders in which the neuroinflammatory component plays a central role, such as MS and AD. FAAH inhibition or melatonin treatment, via pharmacological modulation or genetic ablation, attenuated Aβ accumulation, neuroinflammation and cognitive decline in experimental models of

AD and ameliorated EAE severity and remission in mice (Corpas et al., 2018; Ghareghani et al., 2019; Piro et al., 2012; Rossi et al., 2011; Wen et al., 2016). A relevant result of our study is the finding that UCM1341 was more effective than melatonin or URB597 against the neuroinflammatory insult, and combination of both drugs (each at 10 μM) synergistically halted neurodegeneration with an effect comparable to UCM1341. This suggests that dual-acting compounds may represent a promising approach to treat neuroinflammatory disease states and supports the interplay between the endocannabinoid and melatoninergic systems as an important driver for their beneficial effect. In support, we found that the blockade of PPARα, TRPV1 channels and melatonin receptors, but not of CB_1 and CB_2 receptors, prevented the neuroprotective actions of UCM1341. The fact that the protective effects of UCM1341 were not influenced by the activation of CB receptors is consistent with the observed increase of OEA and AEA levels. OEA exerts a predominant activity through PPARα and TRPV1 channels (Muller et al., 2019). AEA is nearly inactive on CB_2 receptors (Sugiura et al., 2000), a subtype expressed by activated microglia and mediating neuroprotection under neuroinflammation (López et al., 2018). On the other hand, AEA is a partial agonist at CB_1 receptors, but its effect in this model appears to be mediated by TRPV1 channels (Ross, 2003). In support of our findings, the anti-inflammatory response deriving from FAAH inhibition or its knockdown on LPS-stimulated microglia was not reversed by CB_1 or CB_2 receptor antagonists (Tanaka et al., 2019; Tham et al., 2007).

The reason why we were unable to detect an increase in PEA levels is unknown. Previous studies suggested a region-specific alteration in brain NAE levels following inhibition of endocannabinoid degrading enzymes, or it can be possibly due to a time- and spatial-restricted distribution (Bortolato et al., 2007; Henry et al., 2014). On the other hand, PEA hydrolysis is catalysed not only by FAAH but also by the enzyme **N-acylethanolamine acid amidase** (NAAA), whose

---

FIGURE 8 Effect of UCM1341 on the expression of proteins controlling cholesterol metabolism and efflux. Western blot and quantitative densitometric analysis of triggering receptor expressed on myeloid cells-2 (TREM2) (a), liver X receptor (LXR) (b, *left*) and ATP-binding cassette transporter member 1 (ABCA1) (b, *right*) levels in tissue lysates from control and lipopolysaccharide (LPS) + interferon-γ (IFN-γ)-treated explants for 72 h, in the absence or presence of 10 μM UCM1341. Data were normalized on the basis of β-actin levels and expressed as percentage of control. The values shown are the means ± SEM; n = 5. *$P < 0.05$, significantly different from control and LPS + IFN-γ; one-way ANOVA with Bonferroni post hoc analysis. (c) Representative confocal microscopic images showing Iba1 and Plin2 immunoreactivities in the CA1 pyramidal layer under control conditions and LPS + IFN-γ exposure, in the absence or presence of 10 μM UCM1341 for 72 h. Squared areas are shown at higher magnification on the adjacent panel. Arrows point to Iba1^{+}/Plin2^{+} double-labelled cells under UCM1341 exposure. (d) Quantitative analysis of Iba1^{+}/Plin2^{+} cells in control and LPS + IFN-γ-treated cultures, in the absence or presence of 10 μM UCM1341. Data are expressed as the mean number of double-labelled Iba1^{+}/Plin2^{+} cells ± SEM per unit area (mm²) (n = 5). *$P < 0.05$, significantly different from controls and LPS + IFN-γ; one-way ANOVA with Bonferroni post hoc analysis. (e) Representative confocal microscopic images showing Iba1 and ABCA1 immunoreactivities in the CA1 pyramidal region under control conditions and LPS + IFN-γ exposure, in the absence or presence of 10 μM UCM1341 for 72 h. Arrows point to double-labelled Iba1^{+}/ABCA1^{+} cells. (f) Quantitative analysis of Iba1^{+}/ABCA1^{+} cells in control and LPS + IFN-γ-treated cultures, in the absence or presence of 10 μM UCM1341. Data are expressed as the mean number of double-labelled cells ± SEM per unit area (mm²) (n = 5). *$P < 0.05$, significantly different from controls and LPS + IFN-γ; one-way ANOVA with Bonferroni post hoc analysis. (g) Representative confocal microscopic images showing Iba1 and Plin2 immunoreactivities in the CA1 pyramidal region under control conditions, LPS + IFN-γ exposure, LPS + IFN-γ + 10 μM URB597, LPS + IFN-γ + 10 μM melatonin and LPS + IFN-γ + 10 μM URB597 + 10 μM melatonin, for 72 h. Arrows point to double-labelled Iba1^{+}/Plin2^{+} cells. (h) Quantitative analysis of Iba1^{+}/Plin2^{+} cells in control and LPS + IFN-γ-treated cultures, in the absence or presence of 10 μM URB597, 10 μM melatonin and 10 μM URB597 + 10 μM melatonin. Data are expressed as the mean number of double-labelled Iba[+]/Plin2^{+} cells ± SEM per unit area (mm²) (n = 5). *$P < 0.05$, significantly different from controls and LPS + IFN-γ; one-way ANOVA with Bonferroni post hoc analysis. s.p., stratum pyramidale
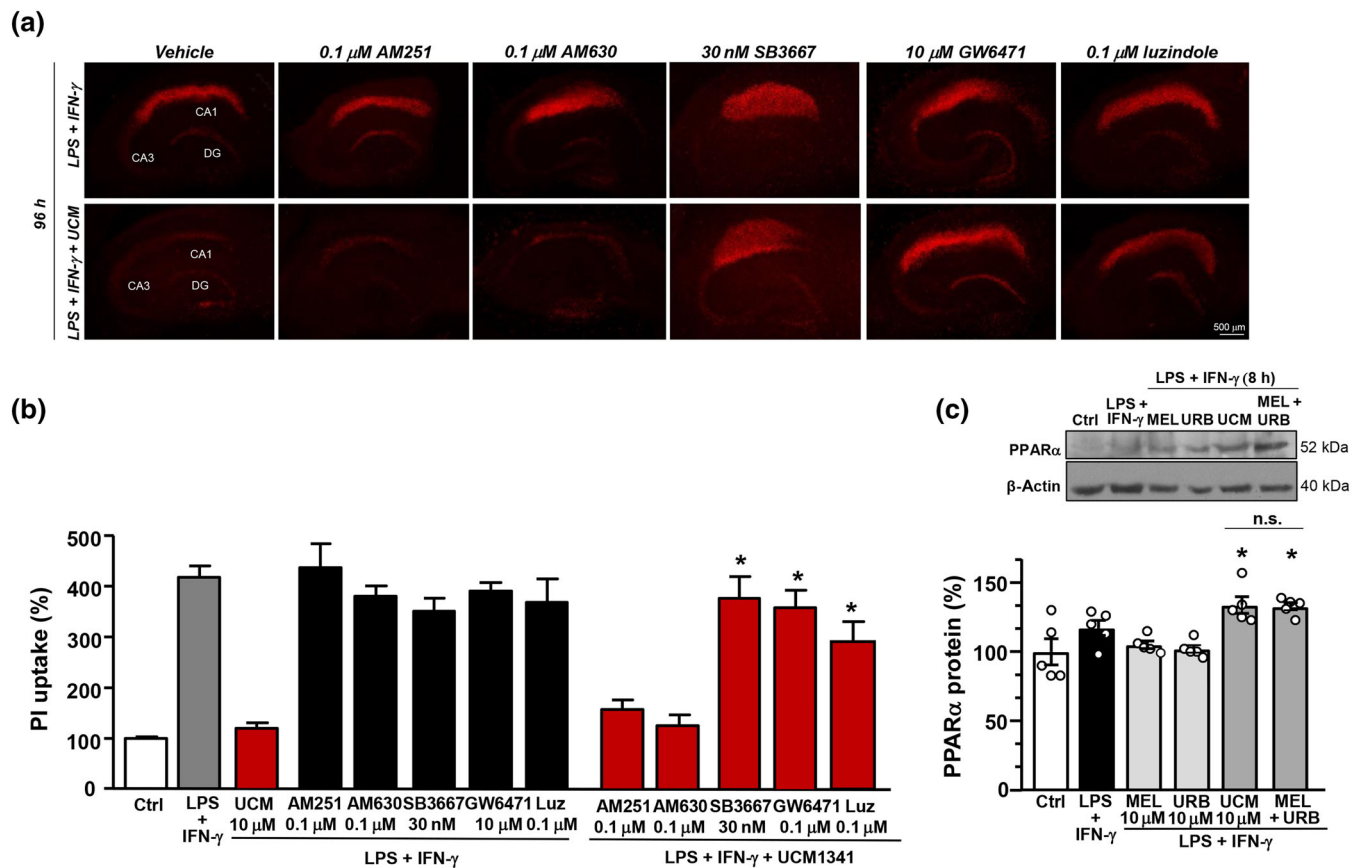
FIGURE 9 Effect of UCM1341 on PPARα levels and of CB1, CB2, TRPV1, PPARα, and melatonin receptor antagonists on drug-induced neuroprotection. (a) Propidium iodide (PI) fluorescence staining patterns observed in hippocampal slice cultures 96 h following lipopolysaccharide (LPS) + interferon-γ (IFN-γ) exposure in the presence of 0.1 μM AM251–CB$_1$ receptor antagonist, 0.1 μM AM630–CB$_2$ receptor antagonist, 30 nM SB3667–TRPV1 channel antagonist, 10 μM GW6471–PPARα antagonist and 0.1 μM luzindole–melatonin receptor antagonist, alone (upper panels) or in combination with 10 μM UCM1341 (lower panels). (b) Quantitative densitometric analysis of PI fluorescence uptake recorded in slices under control conditions, and after LPS + IFN-γ, in the presence of 0.1 μM AM251, 0.1 μM AM630, 30 nM SB3667, 10 μM GW6471 and 0.1 μM luzindole, alone or in combination with 10 μM UCM1341. Data are expressed as percentage of control. The values shown are the means ± SEM; n = 5. *$P < 0.05$, significantly different from UCM1341; one-way ANOVA with Bonferroni post hoc analysis. (c) Protein expression and quantitative densitometric analysis of PPARα in tissue lysates from control and LPS + IFN-γ-treated slices, in the absence or presence of 10 μM melatonin, 10 μM URB597, 10 μM UCM1341 and 10 μM melatonin + 10 μM URB597. Data were normalized on the basis of β-actin levels and expressed as percentage of control. *$P < 0.05$, significantly different from control; n.s., not significant; one-way ANOVA with Bonferroni post hoc analysis.

inhibition in activated inflammatory cells leads to a normalization of PEA levels (Piomelli et al., 2020; Solorzano et al., 2009).

The protective activity of UCM1341 was also counteracted by luzindole, an MT$_1$/MT$_2$ receptor antagonist, implying a receptor-dependent mechanism for the melatoninergic component. Melatonin and related indole derivatives are widely reported as direct antioxidant agents conferring cellular protection from free radical species and pro-oxidant mediators (Reiter et al., 2013). Nevertheless, in hippocampal slices, we observed no effect of UCM1341 on GSH levels and on the balance between the reduced and oxidized species. Recent experimental evidence supports the involvement of melatonin membrane receptors, and in particular of the MT$_1$ subtype, in mediating its neuroprotective activity. Indeed, melatonin receptor activation modulates the activity of transcription factors that in turn decrease the expression of pro-inflammatory mediators, induce antioxidant genes

and promote a shift of microglia towards an M2 phenotype (Zhou et al., 2021). A further support for the receptor-mediated neuroprotective activity of melatoninergic agents comes from the improvement of LPS-induced neuroinflammation exerted by the receptor agonist ramelteon, devoid of the indole nucleus and counteracted by luzindole (Gu et al., 2021).

The synthetic dual agent UCM1341 represents a unique pharmacological tool to investigate the effect of simultaneous activation of melatonin receptors and FAAH inhibition. Dual-acting agents offer potential advantages over drug combinations in terms of higher efficacy, improved tolerance and lower side effects. Additionally, issues related to the different pharmacokinetic profiles of combined drugs, with consequent unbalanced drug exposure, and to drug–drug interactions could be avoided (Proschak et al., 2019). Nevertheless, our results demonstrate the advantage brought by the combined

approach, in which an FAAH inhibitor (URB597) and melatonin are co-administered, implying that the neuroprotective effects of melatonin can be exerted by both receptor- and non-receptor-related mechanisms. A comparison between the therapeutic potential of the combination and of the dual agent would require dose-dependence and in vivo studies. However, in the present study, in all analyses where the comparison was possible, we did not find significant differences between the effects of 10 μM UCM1341 and those of melatonin + URB597 (each at 10 μM).

In support of the synergistic action between the endocannabinoid and melatoninergic systems, we showed that exposure of explants to both UCM1341 and the combined melatonin+ URB597, increased the expression of PPARα levels during the neuroinflammatory insult and favoured the formation of lipid-laden microglia/macrophages. The up-regulation and activation of PPARα contribute to the neuroprotective and anti-inflammatory actions, not only of its endogenous ligand OEA (Sun et al., 2007) but also of melatonin. For instance, Paterniti et al. (2017) showed that the beneficial effects of melatonin on spinal cord tissue injury and pro-inflammatory cytokine release were significantly reduced in PPARα knockout mice.

The central role of TRPV1 channels in glia-to-neuron communication during neuroinflammation has been amply documented (Marrone et al., 2017). Although the consequence of its modulation under neuroinflammatory conditions remains controversial (Boscia et al., 2021), our data support the anti-inflammatory effects of activating TRPV1 channels. Moreover, previous studies showed that PPARα receptors and TRPV1 channels functionally and biochemically interact (Ambrosino et al., 2014), thus suggesting that the cross-talk between these two receptors may also contribute to UCM1341 effects.

PPARα is a ligand-dependent transcription factor that mediates the trans-repression of the main inflammatory transcription factors and acts as a master regulator of lipid metabolism and cholesterol homeostasis (Chinetti et al., 2001). Previous studies have shown that endocannabinoids and some *N*-acylethanolamines, particularly OEA, and melatonin, act as immunomodulators controlling innate immune activation and cytokine release (Chiurchiù et al., 2018). In line, our findings suggest that UCM1341 sustains a pro-resolving macrophage behaviour during neuroinflammation, as reported for both URB597 and melatonin (Grieco et al., 2021; Hardeland, 2021; Mecha et al., 2015; Tanaka et al., 2019). Indeed, in response to the pro-inflammatory insult, the bivalent ligand prevented the release of TNFα, a cytokine mediating the pro-inflammatory activation of microglia, and up-regulated anti-inflammatory macrophage M2 markers. Consistent with the UCM1341-induced synergistic activation of protective endocannabinoid and melatoninergic signalling pathways, we showed that during neuroinflammation, UCM1341 up-regulated the levels of phosphorylated AMP kinase, an important cellular energy sensor that represses pro-inflammatory responses and favours microglia M2 polarization (Trefts & Shaw, 2021).

Recent studies highlighted the complexity of microglia–macrophage subsets during neuroinflammation and revealed an up-regulation of genes involved in phagocytic and lipid metabolism (including TREM2), as well as protective pathways in both disease-associated microglia (DAM) and developmental associated microglia (PAM) (Hammond et al., 2019; Li et al., 2019). Although the characterization of microglial phenotype(s) driven by UCM1341 exposure under neuroinflammation requires further investigation, a recent study revealed that FAAH deletion promoted a DAM-like phenotype in a mouse model of AD (Ruiz-Pérez et al., 2021). On the other hand, the possibility that the use of neonatal animals could have influenced our results appears less likely, as an increased expression of homeostatic microglial genes occurred by 7 DIV in slice cultures, and the exposure to LPS showed prominent similarities with the in vivo response, supporting the emerging consensus that microglial identity in 10–14 DIV slice cultures may model the adult in vivo state (Delbridge et al., 2020; Papageorgiou et al., 2016).

It is now clear that in the absence of proper cholesterol metabolism under conditions of myelin phagocytic activity, macrophages exhibit dysregulated inflammatory responses, phagocyte dysfunction and altered immune functions and tissue regeneration (Berghoff et al., 2021). Our findings, by showing that UCM1341 polarized macrophages to a lipid-laden Plin2+ foamy phenotype and up-regulated the phagocytic receptor TREM2, the lipid-sensing nuclear receptor LXR and the cholesterol efflux transporter ABCA1, suggest a role of the bivalent ligand in providing a restorative response against a neuroinflammatory demyelinating insult through the modulation of cholesterol metabolism. In support, the up-regulation of ABCA1 contributes to the protective and anti-atherosclerotic properties of both OEA and melatonin (Chinetti et al., 2001; Kim et al., 2021).

Collectively, our findings showed that UCM1341, by inhibiting FAAH enzyme and stimulating PPARα, TRPV1 channels and melatonin receptors, modulated the expression of receptors and intracellular signalling pathways governing protective and inflammation resolution responses in the CNS. Further work is needed to determine the effects of joint targeting of the endocannabinoid and melatoninergic systems in models of neurodegenerative disease-associated inflammatory states.

ACKNOWLEDGEMENTS

CONFLICTS OF INTEREST

The authors declare no conflicts of interest.

AUTHOR CONTRIBUTIONS

Mariarosaria Cammarota: Data curation; formal analysis; investigation; methodology; writing-review and editing. **Francesca Ferlenghi:** Formal analysis; investigation; methodology. **Federica Vacondio:** Data

curation; formal analysis; investigation; methodology. **Fabrizio Vincenzi:** Data curation; formal analysis; investigation; methodology; writing-review and editing. **Katia Varani:** Writing-review and editing. **Annalida Bedini:** Investigation. **Silvia Rivara:** Data curation; formal analysis; funding acquisition; investigation; methodology; writing-review and editing. **Marco Mor:** Conceptualization; funding acquisition; writing-review and editing. **Francesca Boscia:** Conceptualization; data curation; formal analysis; funding acquisition; investigation; supervision; writing-original draft; writing-review and editing.

DECLARATION OF TRANSPARENCY AND SCIENTIFIC RIGOUR

This Declaration acknowledges that this paper adheres to the principles for transparent reporting and scientific rigour of preclinical research as stated in the *BJP* guidelines for Design & Analysis, Immunoblotting and Immunochemistry, and Animal Experimentation and as recommended by funding agencies, publishers and other organizations engaged with supporting research.

DATA AVAILABILITY STATEMENT

The data that support the findings of this study are available from the corresponding author upon reasonable request. Some data may not be made available because of privacy or ethical restrictions.

REFERENCES

Adi, N., Mash, D. C., Ali, Y., Singer, C., Shehadeh, L., & Papapetropoulos, S. (2010). Melatonin MT1 and MT2 receptor expression in Parkinson's disease. *Medical Science Monitor*, *16*(2), BR61–BR67. https://doi.org/10.12659/MSM.939088

Alexander, S. P., Christopoulos, A., Davenport, A. P., Kelly, E., Mathie, A., Peters, J. A., Veale, E. L., Armstrong, J. F., Faccenda, E., Harding, S. D., Pawson, A. J., Southan, C., Davies, J. A., Abbracchio, M. P., Alexander, W., al-Hosaini, K., Bäck, M., Barnes, N. M., Bathgate, R., ... Ye, R. D. (2021). The Concise Guide to PHARMACOLOGY 2021/22: G protein-coupled receptors. *British Journal of Pharmacology*, *178*(S1), S27–S156. https://doi.org/10.1111/bph.15538

Alexander, S. P., Cidlowski, J. A., Kelly, E., Mathie, A., Peters, J. A., Veale, E. L., Armstrong, J. F., Faccenda, E., Harding, S. D., Pawson, A. J., Southan, C., Davies, J. A., Coons, L., Fuller, P. J., Korach, K. S., & Young, M. J. (2021). The Concise Guide to PHARMACOLOGY 2021/22: Nuclear hormone receptors. *British Journal of Pharmacology*, *178*(S1), S246–S263. https://doi.org/10.1111/bph.15540

Alexander, S. P., Fabbro, D., Kelly, E., Mathie, A., Peters, J. A., Veale, E. L., Armstrong, J. F., Faccenda, E., Harding, S. D., Pawson, A. J., Southan, C., Davies, J. A., Boison, D., Burns, K. E., Dessauer, C., Gertsch, J., Helsby, N. A., Izzo, A. A., Koesling, D., ... Wong, S. S. (2021). THE CONCISE GUIDE TO PHARMACOLOGY 2021/22: Enzymes. *British Journal of Pharmacology*, *178*(S1), S313–S411. https://doi.org/10.1111/bph.15542

Alexander, S. P., Kelly, E., Mathie, A., Peters, J. A., Veale, E. L., Armstrong, J. F., Faccenda, E., Harding, S. D., Pawson, A. J., Southan, C., Davies, J. A., Amarosi, L., Anderson, C. M. H., Beart, P. M., Broer, S., Dawson, P. A., Hagenbuch, B., Hammond, J. R., Inui, K.-i., ... Verri, T. (2021). THE CONCISE GUIDE TO PHARMACOLOGY 2021/22: Transporters. *British Journal of Pharmacology*, *178*(S1), S412–S513. https://doi.org/10.1111/bph.15543

Alexander, S. P., Mathie, A., Peters, J. A., Veale, E. L., Striessnig, J., Kelly, E., Armstrong, J. F., Faccenda, E., Harding, S. D., Pawson, A. J.,

Southan, C., Davies, J. A., Aldrich, R. W., Attali, B., Baggetta, A. M., Becirovic, E., Biel, M., Bill, R. M., Catterall, W. A., ... Zhu, M. (2021). The Concise Guide to PHARMACOLOGY 2021/22: Ion channels. *British Journal of Pharmacology*, *178*(S1), 57–S245. https://doi.org/10.1111/bph.15539

Alexander, S. P. H., Roberts, R. E., Broughton, B. R. S., Sobey, C. G., George, C. H., Stanford, S. C., Cirino, G., Docherty, J. R., Giembycz, M. A., Hoyer, D., Insel, P. A., Izzo, A. A., Ji, Y., MacEwan, D. J., Mangum, J., Wonnacott, S., & Ahluwalia, A. (2018). Goals and practicalities of immunoblotting and immunohistochemistry: A guide for submission to the British Journal of Pharmacology. *British Journal of Pharmacology*, *175*(3), 407–411. https://doi.org/10.1111/bph.14112

Ambrosino, P., Soldovieri, M. V., De Maria, M., Russo, C., & Taglialatela, M. (2014). Functional and biochemical interaction between PPARα receptors and TRPV1 channels: Potential role in PPARα agonists-mediated analgesia. *Pharmacology Research*, *87*, 113–122. https://doi.org/10.1016/j.phrs.2014.06.015

Benito, C., Núñez, E., Tolón, R. M., Carrier, E. J., Rábano, A., Hillard, C. J., & Romero, J. (2003). Cannabinoid CB$_2$ receptors and fatty acid amide hydrolase are selectively overexpressed in neuritic plaque-associated glia in Alzheimer's disease brains. *Journal of Neuroscience*, *23*(35), 11136–11141. https://doi.org/10.1523/jneurosci.23-35-11136.2003

Benito, C., Romero, J. P., Tolón, R. M., Clemente, D., Docagne, F., Hillard, C. J., Guaza, C., & Romero, J. (2007). Cannabinoid CB$_1$ and CB$_2$ receptors and fatty acid amide hydrolase are specific markers of plaque cell subtypes in human multiple sclerosis. *Journal of Neuroscience*, *27*, 2396–2402. https://doi.org/10.1523/jneurosci.4814-06.2007

Berghoff, S. A., Spieth, L., Sun, T., Hosang, L., Schlaphoff, L., Depp, C., Düking, T., Winchenbach, J., Neuber, J., Ewers, D., Scholz, P., van der Meer, F., Cantuti-Castelvetri, L., Sasmita, A. O., Meschkat, M., Ruhwedel, T., Möbius, W., Sankowski, R., Prinz, M., ... Saher, G. (2021). Microglia facilitate repair of demyelinated lesions via post-squalene sterol synthesis. *Nature Neuroscience*, *24*(1), 47–60. https://doi.org/10.1038/s41593-020-00757-6

Bortolato, M., Mangieri, R. A., Fu, J., Kim, J. H., Arguello, O., Duranti, A., Tontini, A., Mor, M., Tarzia, G., & Piomelli, D. (2007). Antidepressant-like activity of the fatty acid amide hydrolase inhibitor URB597 in a rat model of chronic mild stress. *Biology Psychiatry*, *62*, 1103–1110. https://doi.org/10.1016/j.biopsych.2006.12.001

Boscia, F., Annunziato, L., & Taglialatela, M. (2006). Retigabine and flupirtine exert neuroprotective actions in organotypic hippocampal cultures. *Neuropharmacology*, *51*(2), 283–294. https://doi.org/10.1016/j.neuropharm

Boscia, F., de Rosa, V., Cammarota, M., Secondo, A., Pannaccione, A., & Annunziato, L. (2020). The Na$^+$/Ca^{2+} exchangers in demyelinating diseases. *Cell Calcium*, *85*, 102130. https://doi.org/10.1016/j.ceca.2019.102130

Boscia, F., Elkjaer, M. L., Illes, Z., & Kukley, M. (2021). Altered expression of ion channels in white matter lesions of progressive multiple sclerosis: What do we know about their function? *Frontiers in Cellular Neuroscience*, *15*, 685703. https://doi.org/10.3389/fncel.2021.685703

Boscia, F., Esposito, C. L., Casamassa, A., de Franciscis, V., Annunziato, L., & Cerchia, L. (2013). The isolectin IB4 binds RET receptor tyrosine kinase in microglia. *Journal of Neurochemistry*, *126*(4), 428–436. https://doi.org/10.1111/jnc.12209

Boscia, F., Esposito, C. L., Di Crisci, A., de Franciscis, V., Annunziato, L., & Cerchia, L. (2009). GDNF selectively induces microglial activation and neuronal survival in CA1/CA3 hippocampal regions exposed to NMDA insult through Ret/ERK signalling. *PLoS ONE*, *4*(8), e6486. https://doi.org/10.1371/journal.pone.0006486

Boscia, F., Ferraguti, F., Moroni, F., Annunziato, L., & Pellegrini-Giampietro, D. E. (2008). mGlu1α receptors are co-expressed with CB1 receptors in a subset of interneurons in the CA1 region of organotypic hippocampal slice cultures and adult rat brain.

Neuropharmacology, *55*(4), 428–439. https://doi.org/10.1016/j.neuropharm.2008.04.024

Boscia, F., Passaro, C., Gigantino, V., Perdonà, S., Franco, R., Portella, G., Chieffi, S., & Chieffi, P. (2015). High levels of GPR30 protein in human testicular carcinoma in situ and seminomas correlate with low levels of estrogen receptor-beta and indicate a switch in estrogen responsiveness. *Journal of Cellular Physiology*, *230*(6), 1290–1297. https://doi.org/10.1002/jcp.24864

Cammarota, M., de Rosa, V., Pannaccione, A., Secondo, A., Tedeschi, V., Piccialli, I., Fiorino, F., Severino, B., Annunziato, L., & Boscia, F. (2021). Rebound effects of NCX3 pharmacological inhibition: A novel strategy to accelerate myelin formation in oligodendrocytes. *Biomedicine and Pharmacotherapy*, *143*, 112111. https://doi.org/10.1016/j.biopha.2021.112111

Carnevali, L., Statello, R., Vacondio, F., Ferlenghi, F., Spadoni, G., Rivara, S., Mor, M., & Sgoifo, A. (2020). Antidepressant-like effects of pharmacological inhibition of FAAH activity in socially isolated female rats. *European Neuropsychopharmacology*, *32*, 77–87. https://doi.org/10.1016/j.euroneuro.2019.12.119

Casamassa, A., La Rocca, C., Sokolow, S., Herchuelz, A., Matarese, G., Annunziato, L., & Boscia, F. (2016). Ncx3 gene ablation impairs oligodendrocyte precursor response and increases susceptibility to experimental autoimmune encephalomyelitis. *Glia*, *64*(7), 1124–1137. https://doi.org/10.1002/glia.22985

Chinetti, G., Lestavel, S., Bocher, V., Remaley, A. T., Neve, B., Torra, I. P., Teissier, E., Minnich, A., Jaye, M., Duverger, N., Brewer, H. B., Fruchart, J. C., Clavey, V., & Staels, B. (2001). PPAR-α and PPAR-γ activators induce cholesterol removal from human macrophage foam cells through stimulation of the ABCA1 pathway. *Nature Medicine*, *7*(1), 53–58. https://doi.org/10.1038/83348

Chiurchiù, V., van der Stelt, M., Centonze, D., & Maccarrone, M. (2018). The endocannabinoid system and its therapeutic exploitation in multiple sclerosis: Clues for other neuroinflammatory diseases. *Progress in Neurobiology*, *160*, 82–100. https://doi.org/10.1016/j.pneurobio.10.007

Clapper, J. R., Vacondio, F., King, A. R., Duranti, A., Tontini, A., Silva, C., Sanchini, S., Tarzia, G., Mor, M., & Piomelli, D. (2009). A second generation of carbamate-based fatty acid amide hydrolase inhibitors with improved activity in vivo. *ChemMedChem: Chemistry Enabling Drug Discovery*, *4*(9), 1505–1513. https://doi.org/10.1002/cmdc.200900210

Corpas, R., Griñán-Ferré, C., Palomera-Ávalos, V., Porquet, D., García de Frutos, P., Franciscato Cozzolino, S. M., Rodríguez-Farré, E., Pallàs, M., Sanfeliu, C., & Cardoso, B. R. (2018). Melatonin induces mechanisms of brain resilience against neurodegeneration. *Journal of Pineal Research*, *65*(4), e12515. https://doi.org/10.1111/jpi.12515

Curtis, M. J., Alexander, S., Cirino, G., Docherty, J. R., George, C. H., Giembycz, M. A., Hoyer, D., Insel, P. A., Izzo, A. A., Ji, Y., MacEwan, D. J., Sobey, C. G., Stanford, S. C., Teixeira, M. M., Wonnacott, S., & Ahluwalia, A. (2018). Experimental design and analysis and their reporting II: Updated and simplified guidance for authors and peer reviewers. *British Journal of Pharmacology*, *175*(7), 987–993. https://doi.org/10.1111/bph.14153

de Rosa, V., Secondo, A., Pannaccione, A., Ciccone, R., Formisano, L., Guida, N., Crispino, R., Fico, A., Polishchuk, R., D'Aniello, A., Annunziato, L., & Boscia, F. (2019). D-Aspartate treatment attenuates myelin damage and stimulates myelin repair. *EMBO Molecular Medicine*, *11*(1), e9278. https://doi.org/10.15252/emmm.201809278

Delbridge, A. R. D., Huh, D., Brickelmaier, M., Burns, J. C., Roberts, C., Challa, R., Raymond, N., Cullen, P., Carlile, T. M., Ennis, K. A., Liu, M., Sun, C., Allaire, N. E., Foos, M., Tsai, H. H., Franchimont, N., Ransohoff, R. M., Butts, C., & Mingueneau, M. (2020). Organotypic brain slice culture microglia exhibit molecular similarity to acutely-isolated adult microglia and provide a platform to study neuroinflammation. *Frontiers in Cellular Neuroscience*, *14*, 592005. https://doi.org/10.3389/fncel.2020.592005

Franklin, R. J. M., & Ffrench-Constant, C. (2017). Regenerating CNS myelin—From mechanisms to experimental medicines. *Nature Review Neuroscience*, *18*(12), 753–769. https://doi.org/10.1038/nrn.2017.136

Ghareghani, M., Scavo, L., Jand, Y., Farhadi, N., Sadeghi, H., Ghanbari, A., Mondello, S., Arnoult, D., Gharaghani, S., & Zibara, K. (2019). Melatonin therapy modulates cerebral metabolism and enhances remyelination by increasing PDK4 in a mouse model of multiple sclerosis. *Frontiers in Pharmacology*, *10*, 147. https://doi.org/10.3389/fphar.2019.00147

Gouna, G., Klose, C., Bosch-Queralt, M., Liu, L., Gokce, O., Schifferer, M., Cantuti-Castelvetri, L., & Simons, M. (2021). TREM2-dependent lipid droplet biogenesis in phagocytes is required for remyelination. *Journal of Experimental Medicine*, *218*(10), e20210227. https://doi.org/10.1084/jem.20210227

Grieco, M., De Caris, M. G., Maggi, E., Armeli, F., Coccurello, R., Bisogno, T., D'Erme, M., Maccarrone, M., Mancini, P., & Businaro, R. (2021). Fatty acid amide hydrolase (FAAH) inhibition modulates amyloid-beta-induced microglia polarization. *International Journal of Molecular Sciences*, *22*, 771. https://doi.org/10.3390/ijms22147711

Gu, C., Wang, F., Zhang, Y. T., Wei, S. Z., Liu, J. Y., Sun, H. Y., Wang, G. H., & Liu, C. F. (2021). Microglial MT1 activation inhibits LPS-induced neuroinflammation via regulation of metabolic reprogramming. *Aging Cell*, *20*(6), e13375. https://doi.org/10.1111/acel.13375

Gulyas, A. I., Cravatt, B. F., Bracey, M. H., Dinh, T. P., Piomelli, D., Boscia, F., & Freund, T. F. (2004). Segregation of two endocannabinoid-hydrolyzing enzymes into pre- and postsynaptic compartments in the rat hippocampus, cerebellum and amygdala. *European Journal of Neuroscience*, *20*(2), 441–458. https://doi.org/10.1111/j.1460-9568.2004.03428.x

Hammond, T. R., Dufort, C., Dissing-Olesen, L., Giera, S., Young, A., Wysoker, A., Walker, A. J., Gergits, F., Segel, M., Nemesh, J., Marsh, S. E., Saunders, A., Macosko, E., Ginhoux, F., Chen, J., Franklin, R. J. M., Piao, X., McCarroll, S. A., & Stevens, B. (2019). Single-cell RNA sequencing of microglia throughout the mouse lifespan and in the injured brain reveals complex cell-state changes. *Immunity*, *50*(1), 253–271.e6. https://doi.org/10.1016/j.immuni.2018.11.004

Hardeland, R. (2021). Melatonin and microglia. *International Journal of Molecular Sciences*, *22*(15), 8296. https://doi.org/10.3390/ijms22158296

Henry, R. J., Kerr, D. M., Finn, D. P., & Roche, M. (2014). FAAH-mediated modulation of TLR3-induced neuroinflammation in the rat hippocampus. *Journal of Neuroimmunology*, *276*(1–2), 126–134. https://doi.org/10.1016/j.jneuroim.2014.09.002

Irving, A., Abdulrazzaq, G., Chan, S. L. F., Penman, J., Harvey, J., & Alexander, S. P. H. (2017). Cannabinoid receptor-related orphan G protein-coupled receptors. *Advances in Pharmacology*, *80*, 223–247. https://doi.org/10.1016/bs.apha.2017.04.004

Jockers, R., Delagrange, P., Dubocovich, M. L., Markus, R. P., Renault, N., Tosini, G., Cecon, E., & Zlotos, D. P. (2016). Update on melatonin receptors: IUPHAR Review 20. *British Journal of Pharmacology*, *173*(18), 2702–2725. https://doi.org/10.1111/bph.13536

Kathuria, S., Gaetani, S., Fegley, D., Valiño, F., Duranti, A., Tontini, A., Mor, M., Tarzia, G., La Rana, G., Calignano, A., Giustino, A., Tattoli, M., Palmery, M., Cuomo, V., & Piomelli, D. (2003). Modulation of anxiety through blockade of anandamide hydrolysis. *Nature Medicine*, *9*(1), 76–81. https://doi.org/10.1038/nm803

Kim, J. S., Jung, Y. H., Lee, H. J., Chae, C. W., Choi, G. E., Lim, J. R., Kim, S. Y., Lee, J. E., & Han, H. J. (2021). Melatonin activates ABCA1 via the BiP/NRF1 pathway to suppress high-cholesterol-induced apoptosis of mesenchymal stem cells. *Stem Cell Research & Therapy*, *12*(1), 114. https://doi.org/10.1186/s13287-021-02181-4

Landucci, E., Mazzantini, C., Lana, D., Davolio, P. L., Giovannini, M. G., & Pellegrini-Giampietro, D. E. (2021). Neuroprotective effects of

cannabidiol but not Δ^9-tetrahydrocannabinol in rat hippocampal slices exposed to oxygen-glucose deprivation: Studies with Cannabis extracts and selected cannabinoids. International Journal of Molecular Sciences, 22(18), 9773. https://doi.org/10.3390/ijms22189773

Li, Q., Cheng, Z., Zhou, L., Darmanis, S., Neff, N. F., Okamoto, J., Gulati, G., Bennett, M. L., Sun, L. O., Clarke, L. E., Marschallinger, J., Yu, G., Quake, S. R., Wyss-Coray, T., & Barres, B. A. (2019). Developmental heterogeneity of microglia and brain myeloid cells revealed by deep single-cell RNA sequencing. Neuron, 101(2), 207–223.e10. https://doi.org/10.1016/j.neuron.2018.12.006

Lilley, E., Stanford, S. C., Kendall, D. E., Alexander, S. P. H., Cirino, G., Docherty, J. R., George, C. H., Insel, P. A., Izzo, A. A., Ji, Y., Panettieri, R. A., Sobey, C. G., Stefanska, B., Stephens, G., Teixeira, M., & Ahluwalia, A. (2020). ARRIVE 2.0 and the British Journal of Pharmacology: Updated guidance for 2020. British Journal of Pharmacology, 177(16), 3611–3616. https://doi.org/10.1111/bph.15178

Liu, L., Labani, N., Cecon, E., & Jockers, R. (2019). Melatonin target proteins: Too many or not enough? Frontiers in Endocrinology, 10, 791. https://doi.org/10.3389/fendo.2019.00791

López, A., Aparicio, N., Pazos, M. R., Grande, M. T., Barreda-Manso, M. A., Benito-Cuesta, I., Vázquez, C., Amores, M., Ruiz-Pérez, G., García-García, E., Beatka, M., Tolón, R. M., Dittel, B. N., Hillard, C. J., & Romero, J. (2018). Cannabinoid CB_2 receptors in the mouse brain: Relevance for Alzheimer's disease. Journal of Neuroinflammation, 15(1), 158. https://doi.org/10.1186/s12974-018-1174-9

Marrone, M. C., Morabito, A., Giustizieri, M., Chiurchiù, V., Leuti, A., Mattioli, M., Marinelli, S., Riganti, L., Lombardi, M., Murana, E., Totaro, A., Piomelli, D., Ragozzino, D., Oddi, S., Maccarrone, M., Verderio, C., & Marinelli, S. (2017). TRPV1 channels are critical brain inflammation detectors and neuropathic pain biomarkers in mice. Nature Communications, 8(1), 15292. https://doi.org/10.1038/ncomms15292

Mecha, M., Feliú, A., Carrillo-Salinas, F. J., Rueda-Zubiaurre, A., Ortega-Gutiérrez, S., García de Sola, R., & Guaza, C. (2015). Endocannabinoids drive the acquisition of an alternative phenotype in microglia. Brain Behavior Immunology, 49, 233–245. https://doi.org/10.1016/j.bbi.2015.06.002

Mikheeva, I. B., Shubina, L., Matveeva, N., Pavlik, L. L., & Kitchigina, V. F. (2017). Fatty acid amide hydrolase inhibitor URB597 may protect against kainic acid-induced damage to hippocampal neurons: Dependence on the degree of injury. Epilepsy Research, 137, 84–94. https://doi.org/10.1016/j.eplepsyres.2017.09.017

Moreno-García, Á., Bernal-Chico, A., Colomer, T., Rodríguez-Antigüedad, A., Matute, C., & Mato, S. (2020). Gene expression analysis of astrocyte and microglia endocannabinoid signaling during autoimmune demyelination. Biomolecules, 10(9), 1228. https://doi.org/10.3390/biom10091228

Muller, C., Morales, P., & Reggio, P. H. (2019). Cannabinoid ligands targeting TRP channels. Frontiers in Molecular Neuroscience, 11, 487. https://doi.org/10.3389/fnmol.2018.00487

Nikolaev, G., Robeva, R., & Konakchieva, R. (2021). Membrane melatonin receptors activated cell signaling in physiology and disease. International Journal of Molecular Sciences, 23(1), 471. https://doi.org/10.3390/ijms23010471

Núñez, E., Benito, C., Tolón, R. M., Hillard, C. J., Griffin, W. S., & Romero, J. (2008). Glial expression of cannabinoid CB_2 receptors and fatty acid amide hydrolase are beta amyloid-linked events in Down's syndrome. Neuroscience, 151(1), 104–110. https://doi.org/10.1016/j.neuroscience

Papageorgiou, I. E., Lewen, A., Galow, L. V., Cesetti, T., Scheffel, J., Regen, T., Hanisch, U. K., & Kann, O. (2016). TLR4-activated microglia require IFN-γ to induce severe neuronal dysfunction and death in situ. Proceedings of the National Academy of Sciences of the United States of America, 113(1), 212–217. https://doi.org/10.1073/pnas.1513853113

Paterniti, I., Campolo, M., Cordaro, M., Impellizzeri, D., Siracusa, R., Crupi, R., Esposito, E., & Cuzzocrea, S. (2017). PPAR-α modulates the anti-inflammatory effect of melatonin in the secondary events of spinal cord injury. Molecular Neurobiology, 54(8), 5973–5987. https://doi.org/10.1007/s12035-016-0131-9

Percie du Sert, N., Hurst, V., Ahluwalia, A., Alam, S., Avey, M. T., Baker, M., Browne, W. J., Clark, A., Cuthill, I. C., Dirnagl, U., Emerson, M., Garner, P., Holgate, S. T., Howells, D. W., Karp, N. A., Lazic, S. E., Lidster, K., MacCallum, C. J., Macleod, M., … Würbel, H. (2020). The ARRIVE guidelines 2.0: Updated guidelines for reporting animal research. PLoS Biology, 18(7), e3000410. https://doi.org/10.1371/journal.pbio.3000410

Petrosino, S., & Di Marzo, V. (2010). FAAH and MAGL inhibitors: Therapeutic opportunities from regulating endocannabinoid levels. Current Opinion in Investigational Drugs, 11(1), 51–62. PMID: 20047159.

Piomelli, D. (2003). The molecular logic of endocannabinoid signalling. Nature Review Neuroscience, 4(11), 873–884. https://doi.org/10.1038/nrn1247

Piomelli, D., & Mabou Tagne, A. (2022). Endocannabinoid-based therapies. Annual Review of Pharmacology and Toxicology, 62, 483–507. https://doi.org/10.1146/annurev-pharmtox-052220-021800

Piomelli, D., Scalvini, L., Fotio, Y., Lodola, A., Spadoni, G., Tarzia, G., & Mor, M. (2020). N-Acylethanolamine acid amidase (NAAA): Structure, function, and inhibition. Journal of Medicinal Chemistry, 63(14), 7475–7490. https://doi.org/10.1021/acs.jmedchem.0c00191

Piro, J. R., Benjamin, D. I., Duerr, J. M., Pi, Y., Gonzales, C., Wood, K. M., Schwartz, J. W., Nomura, D. K., & Samad, T. A. (2012). A dysregulated endocannabinoid-eicosanoid network supports pathogenesis in a mouse model of Alzheimer's disease. Cell Reports, 1, 61723. https://doi.org/10.1016/j.celrep.2012.05.001

Proschak, E., Stark, H., & Merk, D. (2019). Polypharmacology by design: A medicinal chemist's perspective on multitargeting compounds. Journal of Medicinal Chemistry, 62(2), 420–444. https://doi.org/10.1021/acs.jmedchem.8b00760

Reiter, R. J., Tan, D. X., Rosales-Corral, S., & Manchester, L. C. (2013). The universal nature, unequal distribution and antioxidant functions of melatonin and its derivatives. Mini Reviews in Medicinal Chemistry, 13(3), 373–384. https://doi.org/10.2174/1389557511313030006

Ross, R. A. (2003). Anandamide and vanilloid TRPV1 receptors. British Journal of Pharmacology, 140(5), 790–801. https://doi.org/10.1038/sj.bjp.0705467

Rossi, S., Furlan, R., De Chiara, V., Muzio, L., Musella, A., Motta, C., Studer, V., Cavasinni, F., Bernardi, G., Martino, G., Cravatt, B. F., Lutz, B., Maccarrone, M., & Centonze, D. (2011). Cannabinoid CB1 receptors regulate neuronal TNF-α effects in experimental autoimmune encephalomyelitis. Brain, Behavior, and Immunity, 25(6), 1242–1248. https://doi.org/10.1016/j.bbi.2011.03.017

Ruiz-Pérez, G., Ruiz de Martín Esteban, S., Marqués, S., Aparicio, N., Grande, M. T., Benito-Cuesta, I., Martínez-Relimpio, A. M., Arnanz, M. A., Tolón, R. M., Posada-Ayala, M., Cravatt, B. F., Esteban, J. A., Romero, J., & Palenzuela, R. (2021). Potentiation of amyloid beta phagocytosis and amelioration of synaptic dysfunction upon FAAH deletion in a mouse model of Alzheimer's disease. Journal of Neuroinflammation, 18(1), 223. https://doi.org/10.1186/s12974-021-02276-y

Savaskan, E., Ayoub, M. A., Ravid, R., Angeloni, D., Fraschini, F., Meier, F., Eckert, A., Müller-Spahn, F., & Jockers, R. (2005). Reduced hippocampal MT_2 melatonin receptor expression in Alzheimer's disease. Journal of Pineal Research, 38(1), 10–16. https://doi.org/10.1111/j.1600-079X.2004.00169.x

Savaskan, E., Olivieri, G., Meier, F., Brydon, L., Jockers, R., Ravid, R., Wirz-Justice, A., & Müller-Spahn, F. (2002). Increased melatonin 1a-receptor immunoreactivity in the hippocampus of Alzheimer's disease patients. Journal of Pineal Research, 32(1), 59–62. https://doi.org/10.1034/j.1600-079x.2002.00841.x

Solorzano, C., Zhub, C., Battista, N., Astarita, G., Lodolae, A., Rivara, S., Mor, M., Russo, R., Maccarrone, M., Antonietti, F., Duranti, A., Tontini, A., Cuzzocrea, S., Tarzia, G., & Piomelli, D. (2009). Selective *N*-acylethanolamine-hydrolyzing acid amidase inhibition reveals a key role for endogenous palmitoylethanolamide in inflammation. *Proceedings of the National Academy of Sciences of the United States of America*, *106*(49), 20966–20971. https://doi.org/10.1073/pnas.0907417106

Spadoni, G., Bedini, A., Furiassi, L., Mari, M., Mor, M., Scalvini, L., Lodola, A., Ghidini, A., Lucini, V., Dugnani, S., Scaglione, F., Piomelli, D., Jung, K. M., Supuran, C. T., Lucarini, L., Durante, M., Sgambellone, S., Masini, E., & Rivara, S. (2018). Identification of bivalent ligands with melatonin receptor agonist and fatty acid amide hydrolase (FAAH) inhibitory activity that exhibit ocular hypotensive effect in the rabbit. *Journal of Medicinal Chemistry*, *61*(17), 7902–7916. https://doi.org/10.1021/acs.jmedchem.8b00893

Sugiura, T., Kondo, S., Kishimoto, S., Miyashita, T., Nakane, S., Kodaka, T., Suhara, Y., Takayama, H., & Waku, K. (2000). Evidence that 2-arachidonoylglycerol but not *N*-palmitoylethanolamine or anandamide is the physiological ligand for the cannabinoid CB2 receptor. Comparison of the agonistic activities of various cannabinoid receptor ligands in HL-60 cells. *The Journal of Biological Chemistry*, *275*, 605–612. https://doi.org/10.1074/jbc.275.1.605

Sun, Y., Alexander, S. P., Garle, M. J., Gibson, C. L., Hewitt, K., Murphy, S. P., Kendall, D. A., & Bennett, A. J. (2007). Cannabinoid activation of PPARα; a novel neuroprotective mechanism. *British Journal of Pharmacology*, *152*(5), 734–743. https://doi.org/10.1038/sj.bjp.0707478

Tanaka, M., Yagyu, K., Sackett, S., & Zhang, Y. (2019). Anti-inflammatory effects by pharmacological inhibition or knockdown of fatty acid amide hydrolase in BV2 microglial cells. *Cell*, *8*, 491. https://doi.org/10.3390/cells8050491

Tham, C.-S., Whitaker, J., Luo, L., & Webb, M. (2007). Inhibition of microglial fatty acid amide hydrolase modulates LPS stimulated release of inflammatory mediators. *FEBS Letters*, *581*, 2899–2904. https://doi.org/10.1016/j.febslet.2007.05.037

Trefts, E., & Shaw, R. J. (2021). AMPK: Restoring metabolic homeostasis over space and time. *Molecular Cell*, *81*(18), 3677–3690. https://doi.org/10.1016/j.molcel.2021.08.015

Vecchiarelli, H. A., Morena, M., Keenan, C. M., Chiang, V., Tan, K., Qiao, M., Leitl, K., Santori, A., Pittman, Q. J., Sharkey, K. A., & Hill, M. N. (2021). Comorbid anxiety-like behavior in a rat model of colitis is mediated by an upregulation of corticolimbic fatty acid amide hydrolase. *Neuropsychopharmacology*, *46*(5), 992–1003. https://doi.org/10.1038/s41386-020-00939-7

Vincenzi, F., Ravani, A., Pasquini, S., Merighi, S., Gessi, S., Setti, S., Cadossi, R., Borea, P. A., & Varani, K. (2017). Pulsed electromagnetic field exposure reduces hypoxia and inflammation damage in neuron-like and microglial cells. *Journal of Cellular Physiology*, *232*(5), 1200–1208. https://doi.org/10.1002/jcp.25606

Wen, J., Ariyannur, P. S., Ribeiro, R., Tanaka, M., Moffett, J. R., Kirmani, B. F., Namboodiri, A. M., & Zhang, Y. (2016). Efficacy of *N*-acetylserotonin and melatonin in the EAE model of multiple sclerosis. *Journal of Neuroimmune Pharmacology*, *11*(4), 763–773. https://doi.org/10.1007/s11481-016-9702-9

Zhang, Y., Cook, A., Kim, J., Baranov, S. V., Jiang, J., Smith, K., Cormier, K., Bennett, E., Browser, R. P., Day, A. L., Carlisle, D. L., Ferrante, R. J., Wang, X., & Friedlander, R. M. (2013). Melatonin inhibits the caspase-1/cytochrome *c*/caspase-3 cell death pathway, inhibits MT1 receptor loss and delays disease progression in a mouse model of amyotrophic lateral sclerosis. *Neurobiology of Disease*, *55*, 26–35. https://doi.org/10.1016/j.nbd.2013.03.008

Zhou, Q., Lin, L., Wang, H., Jiang, S., Huang, P., Lin, Q., Chen, X., & Deng, Y. (2021). Melatonin reduces neuroinflammation and improves axonal hypomyelination by modulating M1/M2 microglia polarization via JAK2-STAT3-telomerase pathway in postnatal rats exposed to lipopolysaccharide. *Molecular Neurobiology*, *58*(12), 6552–6576. https://doi.org/10.1007/s12035-021-02568-7

SUPPORTING INFORMATION

Additional supporting information can be found online in the Supporting Information section at the end of this article.